Vertical electropolishing for 1.3 GHz single- and nine-cell superconducting niobium cavities: A parametric optimization and rf performance

Vijay Chouhan,[1,*] Shigeki Kato,[2] Keisuke Nii,[1] Takanori Yamaguchi,[1] Motoaki Sawabe,[2] Takayuki Saeki,[2] Hideaki Monjushiro,[2] Hiroki Oikawa,[3] Hayato Ito,[4] Hitoshi Hayano,[2] and Yoshiaki Ida[1]

[1]*Marui Galvanizing Co., Ltd., Himeji 272-8022, Japan*
[2]*High Energy Accelerator Research Organization (KEK), Tsukuba 305-0801, Japan*
[3]*Utsunomiya University, Utsunomiya 321-8505, Japan*
[4]*SOKENDAI (The Graduate University for Advanced Studies), Tsukuba 305-0801, Japan*

(Received 29 March 2019; published 3 October 2019)

Electropolishing (EP) is a standard process for the treatment of the interior surface of niobium (Nb) superconducting radio-frequency (SRF) cavities used in particle accelerators. We previously conducted a study on vertical electropolishing (VEP), in which the cavity was set vertically during EP of a 1.3 GHz Nb single-cell cavity. In that study, we showed that the major cause of asymmetric removal in VEP is the accumulation of hydrogen gas bubbles, generated during the EP process, on the upper half cell of the cavity. Three types of unique rotating cathodes were tested with the aim to resolve the issues of asymmetric removal and rough surface. Appropriate cathode design and parameters reduced the asymmetric removal in the cell and yielded a smooth surface of the cavity. In this study, we have performed an extensive investigation on VEP of both single- and nine-cell Nb 1.3 GHz cavities with a modified cathode. The VEP parameters with single- and nine-cell coupon cavities were investigated, which facilitate an *in situ* study of the coupon currents at various positions of the cavities and observation from the viewports located near the iris and equator positions of the cavities. The modified cathode and optimized VEP process for the single-cell cavity yielded uniform removal in the cavity cell and a smooth surface of the interior of the cavity. A novel acid flow method that allows the separation of the acid flow in the cavity and cathode housing was employed in the nine-cell cavity to efficiently remove the gas bubbles from the cavity. The optimized acid flow rates in the cavity and cathode housing, along with other adequate parameters including temperature, cathode rotation speed, and applied voltage, made the surface smooth and significantly reduced the removal nonuniformity in the nine-cell cavity. The single- and nine-cell cavities after an average removal of 46 and 130 μm, respectively, were tested in a vertical cryostat. The single- and nine-cell cavities achieved 31 MV/m at a Q_0 value of 9×10^9 and 28.3 MV/m at a Q_0 value of 6.7×10^9, respectively, in the rf tests at the temperature of 2 K. The achieved SRF performances were as good as the baseline performances achieved after the horizontal electropolishing process of the same cavities.

DOI: 10.1103/PhysRevAccelBeams.22.103101

I. INTRODUCTION

Niobium (Nb) superconducting radio-frequency (SRF) cavities are used in particle accelerators [1] such as the Spallation Neutron Source at Oak Ridge National Laboratory, Continuous Electron Beam Accelerator Facility (CEBAF) at Jefferson Lab, European X-ray Free Electron Laser (XFEL), and other proposed accelerators. A good SRF performance of the cavity is attained with a damage- and contaminant-free smooth surface in the interior of the cavity. The top 100–200−μm-thick surface layer, which is damaged when the cavity is formed, is removed by surface chemistry including buffered chemical polishing (BCP) or electropolishing (EP) [2]. BCP is performed in an acid solution of phosphoric acid (H_3PO_4), nitric acid (HNO_3), and hydrofluoric acid (HF) in a volumetric ratio of 1:1:1 or 2:1:1 [3]. The EP process, which was first introduced for cavity treatment by Ref. [4], is performed in an acid solution of sulfuric acid (H_2SO_4) and HF in a volumetric ratio of 9:1 and with a counter cathode electrode made of pure aluminum [5]. The HF acid is responsible for the removal of the Nb material in both BCP and EP [6]. In BCP, the Nb material is removed

*Corresponding author.
vchouhan@e-marui.jp, vchouhan@post.kek.jp

by chemical etching of the surface in the acid solution. In the EP process, the surface removal occurs under the current limiting condition in which fluorine ions (F^-) from HF diffuse through a diffusion layer lying on the interface of the Nb surface and the electrolyte [7–10]. The F^- ions react with niobium oxide to dissolve the Nb material [7–10]. The EP process shows superiority over the BCP process. The EP process yields a smooth surface as compared to that obtained with the BCP process [11]. Moreover, the EP process results in a better SRF performance of the cavities as compared to that achieved with the BCP process [5,11–15]. Specifically, the BCP process leads to a high field Q slope in a quality factor (Q_0) versus accelerating field (E_{acc}) curve [16,17] and quenching of the cavities at lower fields compared to that with the EP process [13]. A high field Q slope in a $Q_0(E_{\mathrm{acc}})$ curve is observed after both BCP and EP. However, the Q slope can be efficiently removed only from the electropolished (EPed) cavities [17]. A rough surface, although not only this, with sharp steps on the grain boundaries [18] with BCP is considered to be responsible for the limiting SRF performance of the cavity [19]. The EP process is therefore preferred for surface treatment of high gradient Nb cavities. The EP process was successfully employed to the cavities used in accelerator machines like CEBAF and the European XFEL machine.

EP of the accelerating cavities is generally performed in horizontal posture, and, hence, it is called horizontal electropolishing (HEP), a technique developed at the KEK in Japan [1,20]. Before development of the HEP setup, the cavity was also EPed in its vertical position at the KEK [12]. However, the HEP was preferred over the vertical EP (VEP) process, because, in the case of the latter, the generated hydrogen (H_2) gas bubbles on the cathode left bubble traces on the cavity surface [12]. The HEP, therefore, has been adopted as a successful method worldwide [7,21–24]. The effect of this method has been proven by good SRF performances of the approximately 800 Nb elliptical 1.3 GHz cavities used in the European XFEL machine. In contrast, the HEP process requires a massive and expensive setup to rotate the cavity in the EP process, to turn the whole bulky setup in the horizontal posture, and to finally put the cavity in the vertical posture for the acid drainage and post-EP rinsing with water. A simple and cost-effective VEP system was developed at Cornell University to treat the single- and nine-cell cavities [25,26]. Cornell University used a rotating cathode equipped with paddles for agitation of the electrolyte in the cavity cell and a cathode bag for guiding the gas bubbles along the cathode [26–28]. The 1.3 GHz Nb nine-cell cavities showed good SRF performances after VEP, with an average field gradient (E) of 30 ± 6 MV/m and a quality factor (Q_0) of $(1.7 \pm 2) \times 10^{10}$ at 2 K [28]. VEP facilities were also developed in other laboratories [29,30]. The simple VEP setup and rf results have attracted the interest of researchers, as it can be used for minimizing the cost of large-scale projects such as the proposed International Linear Collider (ILC), which will require ~9000 1.3 GHz nine-cell Nb SRF cavities. Besides the HF acid-based VEP, to reduce the cost of the surface treatment and make the treatment environmentally friendly, the bipolar EP, based on reverse pulse voltage and HF acid-free, is also under research and development [31–33].

Although the VEP process is performed with a simple and cost-effective system, it usually results in a longitudinal asymmetry in the removal and rough surface with bubble stripes [28,34,35]. To make the removal symmetric, VEP is performed in two sequences, and the cavity is flipped in the second sequence of the VEP. The process is, therefore, time consuming. Efforts have been made to reduce the nonuniformity in the removal using different shapes of the cathode to obtain a uniform acid flow [34] and electric field [36] on the surface of the cavity cell. However, the aforementioned issues have not been resolved.

We are therefore still investigating VEP to perform it without turning the cavity upside down for symmetric removal. We have earlier reported [35] that the asymmetric removal is supposed to be mainly the result of an accumulation of H_2 gas bubbles on the upper half cell of a single-cell cavity [35]. The bubbles hitting the Nb surface might alter the diffusion layer to enhance the EP current and removal rate. To reduce bubble accumulation, different versions of our patented unique cathode, called the Ninja cathode, were used on the single-cell cavity [35]. The cathode rotation at an adequate speed reduced the removal asymmetry to a great extent. However, the removal asymmetry was still present with 1.5 times higher removal near the top iris compared to that near the bottom iris. The effect of cathode design was also studied by measuring the polarization curves, which are the curves of a current density (J) against an applied voltage (V). A polarization curve represents the current limiting plateau when the diffusion condition, in which EP should be performed, is satisfied [35]. The curves explained the cavity's surface morphologies after VEP under different conditions [35]. The EP process on the Nb surface has been extensively studied to understand the mechanism and its effect on the surface contamination. However, the aforementioned studies were mainly performed at the laboratory scale with small samples of Nb and single-cell cavities [8–10,25,35–39]. A systematic parametric study of the nine-cell cavity to understand the effect of VEP parameters at different positions of the cavity has not been performed, and the VEP conditions are yet to be optimized for achieving uniform removal and a smooth surface. Here, we intend to present a detailed VEP parametric study with a modified Ninja cathode for single- and nine-cell cavities, novel approaches for acid flow, the cavity performance in rf tests, and comparisons of VEP results with those achieved with the standard HEP process.

II. EXPERIMENTAL SETUP

A. Ninja cathode

Three types of Ninja cathodes, namely, NC-1, NC-2, and NC-3, were presented earlier [35]. The NC-3 was prepared with partial metal blades to maintain the cathode near the equator position. The partial metal blades showed an advantage over the insulating blades of the NC-2, as the former yield a smooth equator surface at the same applied voltage. The rough equator surface with the NC-2 was attributed to the large anode-cathode distance and cathode screening by gas bubbles that lowered the electric field on the equator [35]. A drawback of using the partial metallic blades is that the generated gas bubbles on the metallic cathode blades accumulate on the upper half cell of the cavity. In the case of the single-cell cavity, the bubble accumulation on the surface was reduced by applying cathode rotation at 50 rpm [35]. However, the NC-3 with partial metal blades is not suitable for VEP of a nine-cell cavity, because the gas bubbles generated on the blades in each cell finally accumulate in an exceptionally large quantity in the upper cells of the cavity.

A new cathode, called NC-4, was designed with four insulating blades as in the NC-2, but the cathode surface area was enlarged to minimize the cathode screening. The cathode surface area, which was less than 10% of the cavity surface area in the NC-2, was enhanced to be approximately 35% by using more Al rods along with the centered Al cathode pipe. The concept of enhancing the cathode surface area is based on our laboratory EP experiments, in which we studied the effect of the cathode to anode surface area ratio and anode-cathode distance on the EP plateaus in polarization curves. In these tests, both the anode-cathode distance and cathode to anode surface area ratio were varied from 2 to 15 cm and 2% to 50%, respectively. It was observed that a large anode-cathode distance leads to a shift in the EP plateau toward the higher voltage side when the cathode to anode surface area ratio is less than ~10%. Additionally, an insulating cathode housing, which has slits for the current flow between the anode and cathode, is covered with a meshed Teflon sheet so as to guide the bubbles inside the cathode housing and reduce the bubble quantity in the cell. The schematic of the cathode is shown in Fig. 1. The cathode is inserted into a cavity, and the blades are expanded in the cavity cell.

B. Coupon cavities

A 1.3 GHz single-cell Nb coupon cavity, as presented earlier [35], was designed to study and optimize the VEP parameters. Similar single-cell cavities have been used earlier for surface analysis after HEP and barrel polishing [40,41]. Six Nb disk coupons with a diameter of 8 mm are set on the beam pipes, near the irises, and the equator positions of the cavity. An EP current is measurable for the individual coupon, where the coupon currents present the EP information at the particular location of the cavity. Moreover, the coupon surfaces after EP provide surface state information of the cavity, which includes surface morphology and contaminants. The surfaces of the coupons can be analyzed with different surface analytical tools for the surface morphology and chemical analyses. The single-cell cavity also contains viewports at the equator and iris positions for *in situ* observation during the EP process. A unique and innovative nine-cell coupon cavity was also designed and fabricated for finding the optimized VEP parameters for multicell cavities. The nine-cell coupon cavity contained a total of nine coupons and six viewports at the equator and near the iris positions of the first, fifth, and ninth cells of the cavity [42]. Figure 2 shows the nine-cell coupon cavity with the coupon and viewport positions. As in the single-cell coupon cavity, the EP currents for the nine coupons can be measured, as the coupons are electrically isolated from the cavity and the H_2 gas bubbles can be observed from the viewports. The coupons in the top (first), center (fifth), and bottom (ninth) cells are compared to find an impact of VEP on the longitudinal positions in the vertical axis. All the coupons used in this study were prepared using the same sheet of fine-grain polycrystalline Nb material, from Tokyo Denkai, with an average grain size of 30 ± 5 μm.

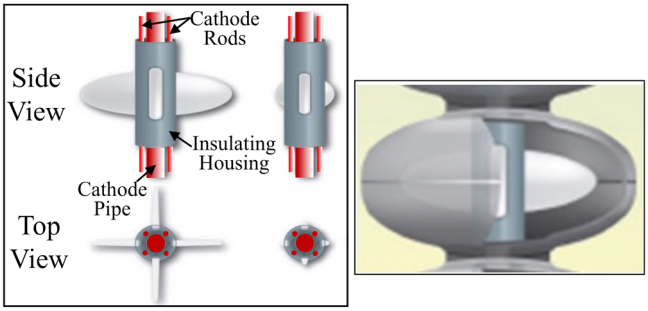

FIG. 1. Schematic of the Ninja cathode with insulating blades, cathode housing, Al cathode axial pipe, and four Al rods in the insulating housing to enhance the cathode surface area. The schematic on the right shows the cathode inside a cavity cell.

C. VEP setup

A VEP setup was designed with a cavity stand with the cavity set in the vertical posture, an acid and water flow unit with program-controlled electric valves, pumps for acid and water, pipelines to flow acid and water from the upside or downside, a touch panel screen to remotely control the flow direction and rates, and interlocks for safety. Figure 3 shows the schematic of the VEP setup. The whole setup was installed in a hall having a floor area of ~25 m^2. The flow rate is measured with a flow meter set at the inlet line. An acid tank with a capacity of 70 L was used. The tank was prepared with meshed filters to reduce the circulation

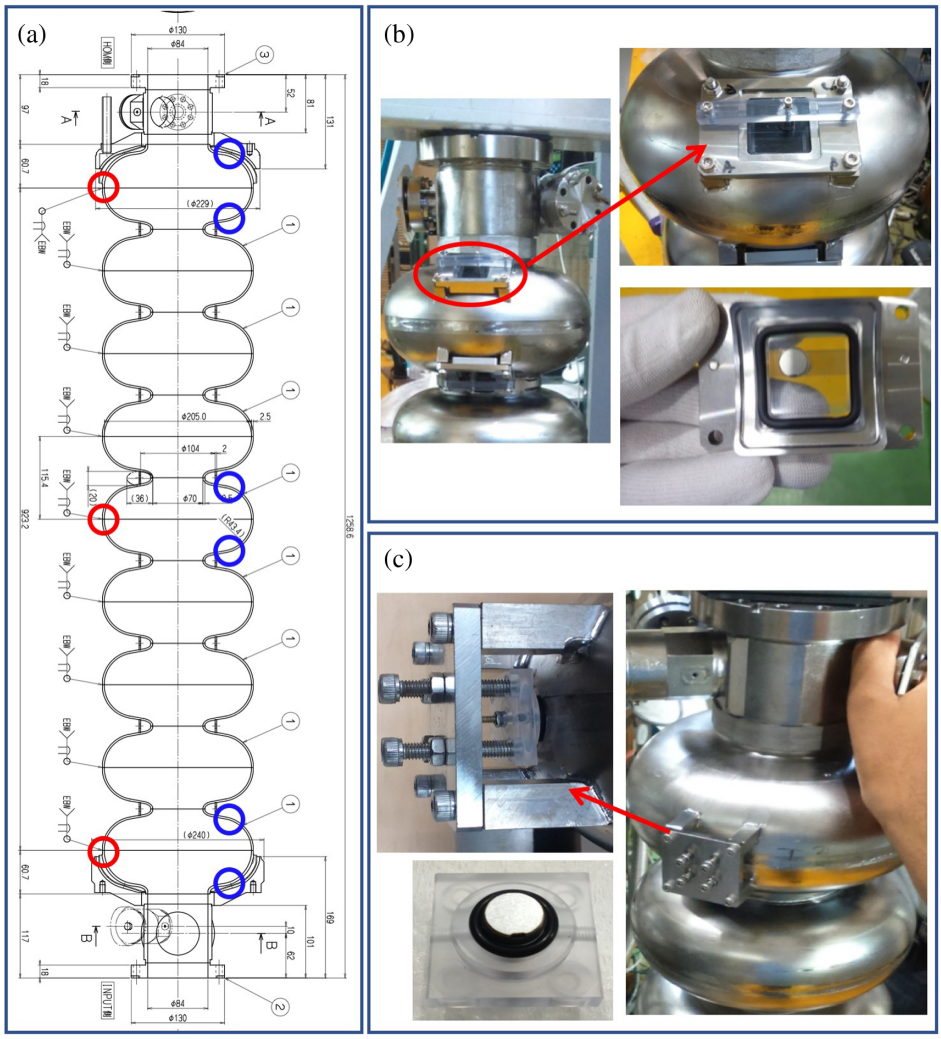

FIG. 2. (a) Diagram of the nine-cell coupon cavity with the nine coupon positions in the first, fifth, and ninth cells as represented with the circles on the cavity drawing. The blue circles represent coupons with viewports near the iris positions. The red circles represent the coupons without viewports at the equator positions. (b) Photographs of one of the iris coupons fixed on the viewport. (c) Equator coupon with the coupon holder.

of H_2 gas bubbles. The operating temperature in the VEP process was maintained by cooling the acid with a heat exchanger set in the acid tank and by spraying water on the exterior of the cavity. The water temperature was controlled by another heat exchanger and a chiller. An ac motor with variable speed was used for the cathode rotation. VEP was performed with a power supply having a rated voltage/current of 20 V/300 A. Temperature sensors were set on the top and bottom beam pipes, top and bottom irises, and the equator positions of a single-cell cavity. In the case of a nine-cell cavity, a total of nine temperature sensors were set on the top iris, bottom iris, and equator of the top, center, and bottom cells. The VEP data including the cavity temperature, acid temperature in the acid tank, EP current, applied voltage, and acid flow rate were logged systematically.

III. RESULTS AND DISCUSSION

A. VEP study with single-cell coupon cavity

The NC-4 was tested first on the single-cell coupon cavity to understand its effect and optimize the VEP parameters for the single-cell cavity. An acid solution of H_2SO_4 (98 wt %) and HF (55 wt %) in a volumetric ratio of 9:1 was circulated at 5–10 L/min in the cavity in the bottom to top direction. Similar to the study performed with the previous Ninja cathodes [35], another was performed with the NC-4 to find an adequate cathode rotation speed. An adequate speed should be able to avoid the accumulation of bubbles on the upper half cell of the cavity to yield similar currents, which represent a similar removal rate. The cathode rotation speed was varied from 0 to 50 rpm in steps of 10 rpm while the top and bottom iris coupon

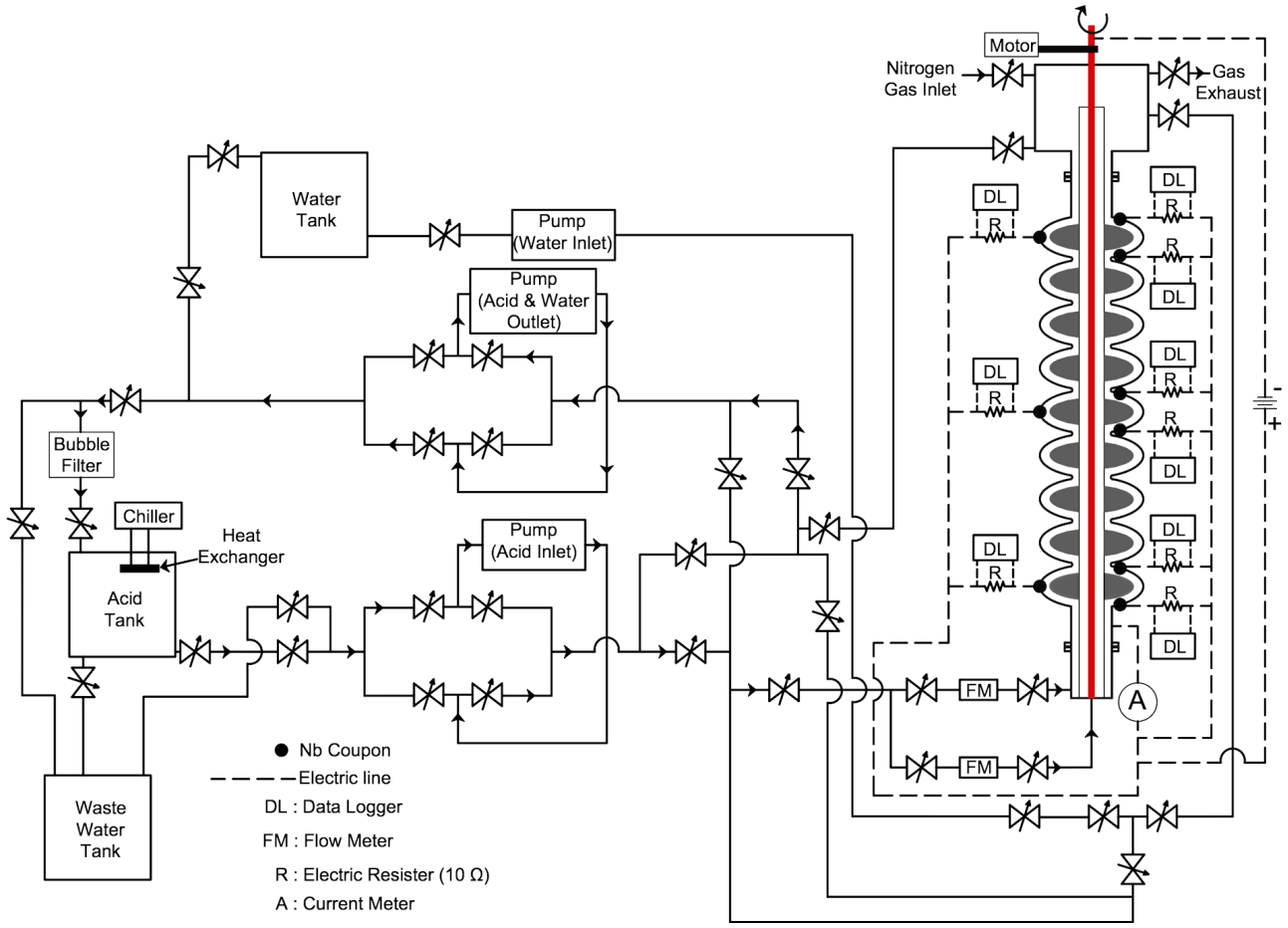

FIG. 3. Schematic of the acid and water flow unit used for VEP and water rinsing of the cavity. The dashed lines represent electric lines connected to the coupons, cavity, and cathode. The arrows indicate the acid flow direction in the VEP process.

currents were monitored. The viewport near the top iris was simultaneously observed to confirm the effect of rotation on accumulation of bubbles. Bubble accumulation in the cell was found to be less with the NC-4 compared to that with the previous model NC-3. This indicated that bubbles moved mainly inside the cathode housing. In this case, a cathode rotation speed of 20 rpm was found to be sufficiently high to stop bubble accumulation on the surface and maintain similar currents for both iris coupons. The cathode rotation speed of 20 rpm was opted for further study.

Polarization curves ($J-V$) were measured for individual coupons and the cavity. The cavity temperature, cathode rotation, and acid flow rate were set to be $\sim 17\,^{\circ}\mathrm{C}$, 20 rpm, and $5-10$ L/ min, respectively. The $J-V$ curves for coupons located at the various positions of the cavity are shown in Figs. 4(a)–4(c), and the $J-V$ curve for the average over the cavity is shown in Fig. 4(d). The EP plateaus were apparently observed for all the coupons and the cavity. The EP plateaus appeared at a higher voltage for the iris and equator coupons as compared to that for the beam pipe coupons. The periodic current oscillations in the VEP process observed from 15 V onward for all the coupons and cavity were found to be independent of the coupon positions and anode-cathode distance. This phenomenon is the same as that reported for HEP and is called extreme diffusion limited EP [7]. The effect of the cathode rotation speed and temperature was also observed on the $J-V$ curves. The EP plateaus for the coupons in the cell, especially at the equator, shifted toward a higher voltage at a higher rotation speed and higher temperature. A slight shift of ~ 1.2 V in the EP plateaus of the iris and equator coupons was noticed due to cathode rotation at 20 rpm. An EP plateau at $\sim 25\,^{\circ}\mathrm{C}$ and 50 rpm produced a voltage shift of more than 3 V compared to that at $17\,^{\circ}\mathrm{C}$ and 20 rpm. Thus, to maintain a clear EP plateau within 20 V, the cavity temperature was preferably selected to be below $20\,^{\circ}\mathrm{C}$ with a cathode rotation of 20 rpm in the VEP process. The effect of the cavity temperature was systematically studied with the nine-cell cavity, as shown in Fig. 18 in Sec. III C below.

The shift in the iris and equator coupons compared to the beam pipe coupons was mainly attributed to a lower electric field on the Nb surface. The electric field was lowered due to cathode screening by gas bubbles and a larger distance

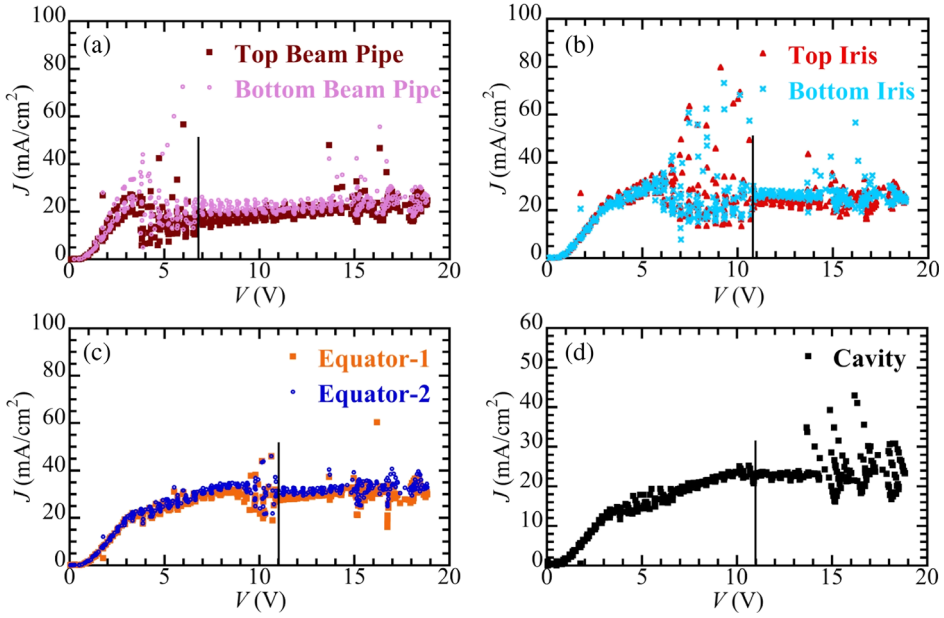

FIG. 4. $J-V$ curves for the coupons (a)–(c) and cavity (d) in the VEP process performed with cathode rotation at 20 rpm, a cavity temperature of 17 °C, and an acid flow rate of 5–10 L/ min. The vertical solid line in each plot represents the start of the EP plateau.

from the cathode especially for the equator. The strong cathode screening shifts the EP plateaus of the Nb surface distant from the cathode. This effect was noticed in the laboratory EP experiment performed for different cathode to anode surface area ratios as stated above in Sec. II A. The shift increased with the increase in the cathode rotation speed. A higher rotation speed enhances the acid flow on the Nb surface, which might physically impair the diffusion layer on the Nb surface in the cavity cell. To form an intact diffusion layer at a higher cathode rotation, a higher voltage might be required. Additionally, a diffusion layer might become thinner owing to a higher acid flow speed at a higher rotation and, thus, result in a rise in the EP current. The current with the cathode rotation at 20 rpm was ∼15% higher than that without the cathode rotation. A higher current at a higher acid flow on a rotating disk electrode was also observed and ascribed to a thin diffusion layer [10] and diffusion of a higher concentration of F^- [9]. The increased current makes the screening of the cathode surface stronger, and the stronger cathode screening further reduces the electric field on the Nb surface. In comparison to the NC-3 [35], the plateau appears at a higher voltage if the same cathode rotation speed of 50 rpm is applied. However, the NC-4 at 20 rpm showed a similar onset voltage, at which the plateau starts to appear, to that of the NC-3 at 50 rpm.

The VEP of the coupon cavity was carried out for an average removal thickness of 28 μm under the optimized parameters listed in Table I. The voltage applied in the VEP process was close to the onset voltage of the plateau in the $J-V$ curves of the equator coupons. The cavity temperature was uniformly maintained below 16 °C with the water spray on the exterior surface of the cavity. The removal rate was estimated to be 0.23 μm/ min at an average current density of ∼17 mA/cm^2.

The effect of the applied VEP parameters was confirmed by observing the coupon surfaces after the VEP with a scanning electron microscope (SEM). SEM images before and after VEP are shown in Fig. 5. The surface roughness Ra and Rz of the coupons was also measured with a mechanical surface profiler in a scanning length of 2.4 mm. Ra is an average of the absolute heights of the surface profile from the mean line, and Rz is defined as the sum of the average absolute values of the five tallest peaks and five deepest valleys from the mean line. Typical Ra and Rz of the as-received coupon surface are 0.6 and 5 μm, respectively. The Ra and Rz of the coupons after the VEP are shown against the coupon position in Fig. 6. Ra and Rz at the equator were lower than 0.2 and 1 μm, respectively. A VEP process performed with the cathode rotation at 50 rpm, a higher temperature (maximum 22 °C), and a voltage of 14 V made the equator surface slightly rougher, with Rz of 2 μm. The images and roughness data reveal that

TABLE I. Conditions for VEP conducted for a single-cell coupon cavity.

Condition	Value
Cathode type	NC-4
Cathode rotation	20 rpm
Cavity temperature	16 °C (preferably below 20 °C)
Voltage	12.5 V
Acid flow rate	5 – 10 L/ min

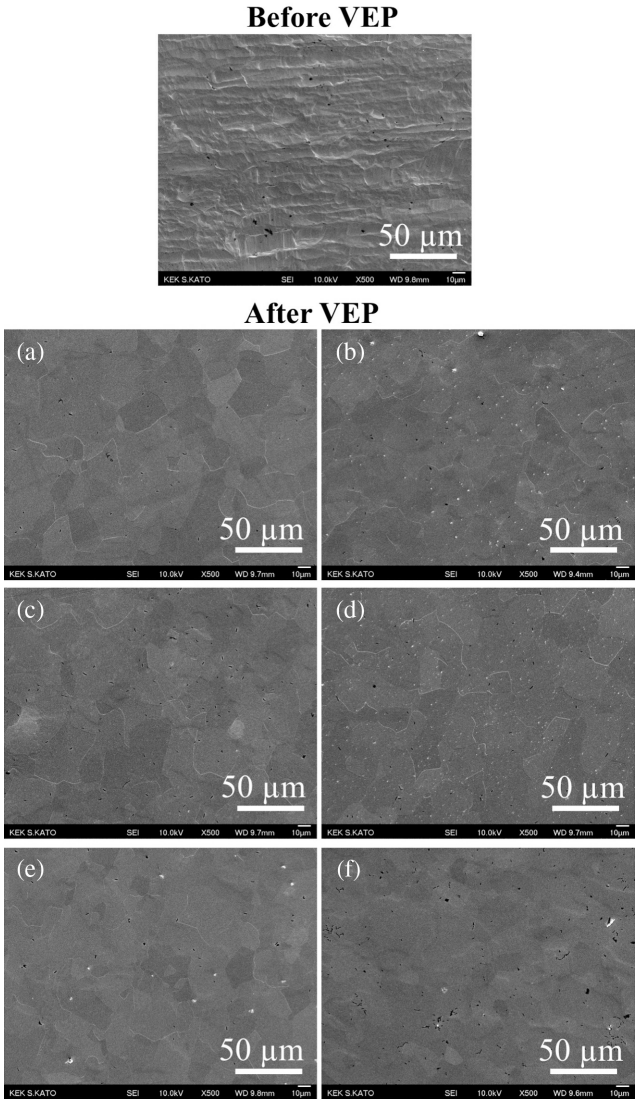

FIG. 5. SEM image of the as-received coupon surface without any surface treatment (top image). SEM images of the coupons located at the (a) top beam pipe, (b) bottom beam pipe, (c) top iris, (d) bottom iris, and (e),(f) equator positions for the VEP performed at 12.5 V, a cathode rotation of 20 rpm, and a maximum cavity temperature of 16 °C.

the VEP process with the applied parameters yielded smooth surfaces in all the coupons. The smooth surfaces in all the coupons were the result of the EP performed in the plateau region. The surface was as smooth as obtained with the NC-3 having the partial metallic blades. The smooth surface validates that the parameters applied in VEP are appropriate for the single-cell cavity.

The removal thickness at various positions of the cavity was measured carefully with an ultrasonic thickness gauge. The removal trend in VEP is compared with that in the HEP, as shown in Fig. 7. The HEP of the cavity was conducted in the superconducting rf test facility (STF) at the KEK, with the STF standard parameters for the single-cell cavity. In the HEP, a cavity rotation of 1 rpm, acid flow

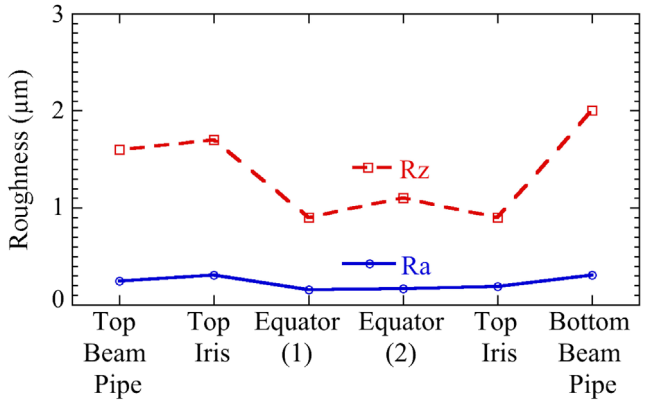

FIG. 6. Surface roughness Ra and Rz of the coupon surfaces after VEP performed at 12.5 V, a cathode rotation of 20 rpm, and a cavity temperature below 16 °C.

rate of 5 L/ min, maximum cavity temperature of ~40 °C, and voltage of 29 V were set. The HEP of the cavity was performed for an average removal of 39 μm at a removal rate of 0.24 μm/ min. The thickness shown in Fig. 7 is an average of three measured values on the same position. The maximum error in the measured thickness appears to be less than ± 5 μm. In both EP processes, the removal trends were symmetric, with the highest removal on both irises. However, the removal in the cell was better in uniformity, with less difference in removal thicknesses between the equator and iris positions in the VEP as compared to that in

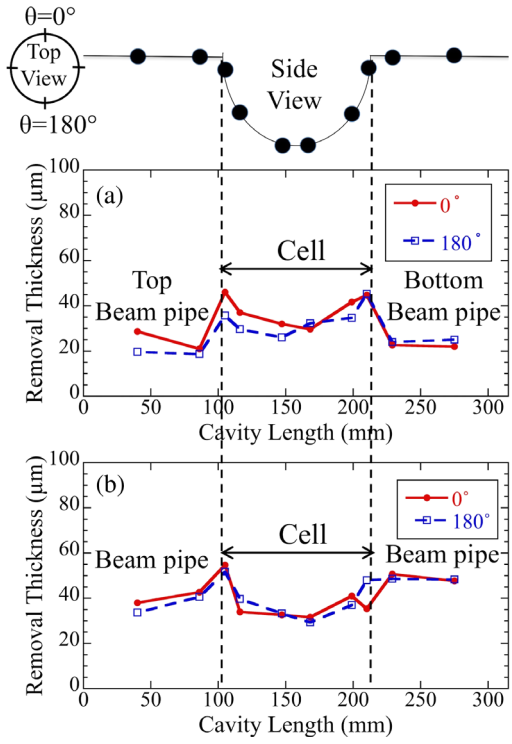

FIG. 7. Trends of the removal thicknesses along the cavity length in the VEP (a) and HEP (b) processes.

the HEP. The symmetric removal in the VEP was a significant improvement over our previous VEP results [35] and those reported by other labs [28,34,35,43,44].

The symmetric removal in the VEP was expected, as both iris coupons showed similar currents under the applied conditions. The symmetric removal trend has revealed the importance of the meshed housing that guided bubbles along the cathode, an adequate acid flow at $5-10$ L/ min that moved the bubbles with a sufficiently high speed to reduce the bubble diffusion into the cavity cell, and the adequate cathode rotation speed. The better symmetry with the NC-4 compared to that with the NC-3 is supposed to be due to the efficient suppression of bubble accumulation and a slower cathode rotation speed of 20 rpm. In the case of the NC-3, bubbles were displaced from the surface only by applying a higher cathode rotation so as to reduce their residence time on the surface. The bubbles might be still hitting the surface. The asymmetry with the NC-3 was also attributed to the turbulent flow created on the top iris by the cathode rotation of 50 rpm [35]. The turbulence might be reduced with NC-4 rotating at a slower rotation of 20 rpm. The higher removal on the irises in both VEP and HEP processes should not be the result of an electric field on the irises, because, in VEP, the electric field remains higher on the beam pipes compared to that near the irises and equator owing to the proximity of the cathode to the beam pipes. The electric field on the surface affects only the onset voltage for the EP plateau in the $J-V$ curves. The EP current remains independent of the electric field in the EP plateau region, in which the VEP was accomplished. A voltage drop may occur mainly in the diffusion layer on the Nb surface [4,7]. This suggests that the difference in the electric field should not create the difference in removal on the equator and irises. The higher removal on the irises might be related to the circulating acid in the cavity. The circulating acid flow might be disrupted at the iris positions to form a higher speed of the acid near the irises. A higher acid flow on the irises was evaluated in the simulation for HEP in which the acid enters to the cavity cell via the cathode pipe and exits from both beam pipes [45]. Eozenou *et al.* also attributed the low removal on the equator in HEP to the slow acid flow [34]. In VEP, a similar phenomenon might also occur. A fluid dynamic simulation in the vertical position of the cavity showed that the acid flow on the irises changes depending on the cathode design [30]. This also needs to be verified by simulating the acid flow with the Ninja cathode. However, the flow speed on the irises could be minimized with a controlled slow flow rate of the circulating acid. The better removal uniformity with less difference between the removal on the irises and equator in the cavity cell in VEP might arise from the cathode rotation, which enhances the acid flow on the cavity cell surface, including the equator.

B. VEP and rf test of single-cell cavity

The VEP result clearly reveals that the optimized VEP process yields a desired smooth surface and removal uniformity. The VEP process was applied to a Tesla shape 1.3 GHz Nb single-cell cavity (TB1-TSB02) to evaluate its rf performance and compare it with a baseline rf result obtained after the HEP process. The cavity was processed with HEP in several steps for a total removal thickness of 280 μm including the last two steps for bulk removal of 100 μm and light removal of 20 μm. The cavity was annealed at 750 °C for 3 h before the final light removal of 20 μm. The cavity was then baked at 120 °C for 48 h and tested in a vertical cryostat at 2 K for the baseline rf performance. The VEP was performed at ∼16.5 V with almost periodic current oscillations, a cavity temperature of ∼19 °C, a controlled acid flow rate of ∼5 L/ min, and a cathode rotation of 20 rpm for an average removal thickness of 36 μm. The voltage of 16.5 V, which was sufficiently higher than the onset voltage, was set to avoid any etching of the equator surface. The current and temperature profiles are shown in Fig. 8(a). The periodic current oscillations, which appeared at the same voltage for all the coupons in the plateau region regardless of the position, guarantee removal of the entire cavity surface under the diffusion-limited regime. The periodic current oscillations might be related to the phenomenon of diffusion of F^- ions and its species through the Nb salt film developed on the Nb surface during the EP process [7,9]. The concentration of F^- ions on the Nb surface periodically changes to remove niobium pentoxide periodically [2,7]. The removal thickness was measured to observe the removal trend along the cavity length. The removal thickness in the cell was almost uniform, and the surface appeared to be smooth. The surface became smoother than that after the HEP treatment. The surface after the VEP was observed with an inspection camera known as the Kyoto camera [46] (see Fig. 8). The improvement in the uniformity compared to that in the coupon cavity is due to a reduction in the removal on the iris positions. The controlled average acid flow rate of ∼5 L/ min in the combination of the cathode rotation might have improved the acid flow uniformity on the cavity cell surface to yield uniform removal in the cell.

A vertical test planned after the VEP for 36 μm could not be conducted, because a vacuum leak occurred at 100 K in the cooldown process in the cryostat. The gas pressure in the cavity increased to be more than 1×10^{-2} Pa, the maximum pressure limit for the ion pump operation and pressure measurement. The cavity was annealed at 750 °C to reset the surface, followed by VEP for 10 μm removal under the same EP conditions. The cavity was baked at 120 °C for 48 h before it was tested at 2 K in the cryostat. The cavity achieved an accelerating gradient of 31 MV/m at Q_0 of 9×10^9 limited by quench. The rf performance

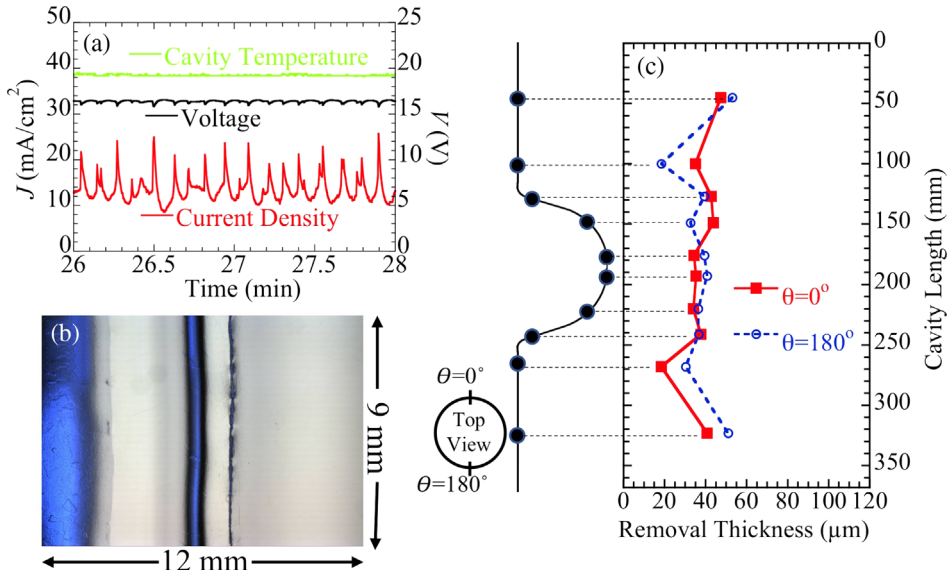

FIG. 8. Current, voltage, and temperature profiles (a) an optical image of the equator weld surface (b) obtained with the Kyoto camera, and the removal thickness trend (c) in the VEP performed for 36 μm average removal.

after the VEP process was as good as that achieved after the HEP process (see Fig. 9).

The surface and rf results show that the optimized VEP process with the Ninja cathode is promising for single-cell cavities and could be an alternative for the HEP process.

C. VEP study with nine-cell cavities

1. VEP with initial parameters

A dedicated NC-4 was also prepared for VEP treatments of nine-cell cavities. A Tesla shape nine-cell cavity (TB9-TSB02), which was previously treated with HEP for 100 μm removal, was treated with VEP under initial parameters similar to those optimized with the single-cell cavity. The applied parameters for VEP are listed in Table II. An average current density of 22 mA/cm^2 was recorded. The VEP was performed for an average removal of 51 μm with a removal rate of 0.28 μm/ min.

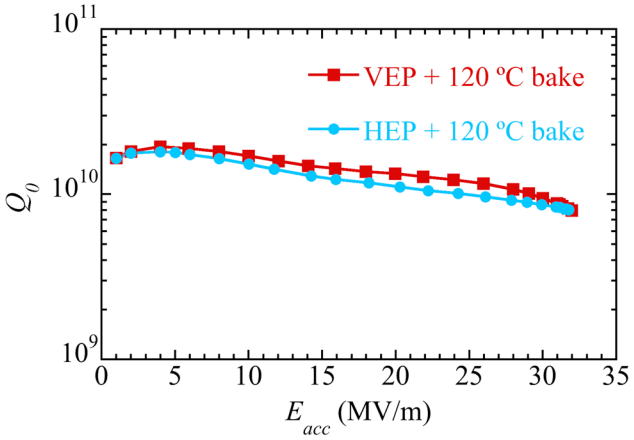

FIG. 9. Comparison of the quality factor (Q_0) versus accelerating field (E_{acc}) curves measured at 2 K after VEP and HEP of a Tesla-shape 1.3 GHz single-cell Nb cavity. SRF tests were conducted after HEP performed for bulk removal and final light removal of 20 μm, and VEP performed for removal of 36 μm and final light removal of 10 μm. Baking at 120 °C for 48 h was applied after the final light removals.

An optical inspection of the equator surface was carried out with the Kyoto camera. The images of the equator surface in all the cells are shown in Fig. 10. Although the entire exterior cavity surface has a uniform temperature maintained with the water spray, it was interesting to observe that the equator surface was rougher only in the top four cells (cells 1–4). The roughness increased toward the top cell.

The removal trend in the VEP in Fig. 11 shows strong nonuniform removal along the cavity length and within the top five cells. The excessive removal was measured in the upper half of the top five cells. The VEP parameters optimized with the single-cell cavity were found to be inappropriate for VEP of the nine-cell scale cavity to yield the desired EPed surface and removal uniformity for the entire cavity. However, these parameters seem to provide a smooth surface and uniform removal for a four-cell scale cavity.

TABLE II. Initial VEP conditions applied to the nine-cell cavity TB9-TSB02.

Condition	Value
Cathode type	NC-4
Cathode rotation	20 rpm
Cavity temperature	15–22 °C
Voltage	15 V
Acid flow rate	~5 L/ min

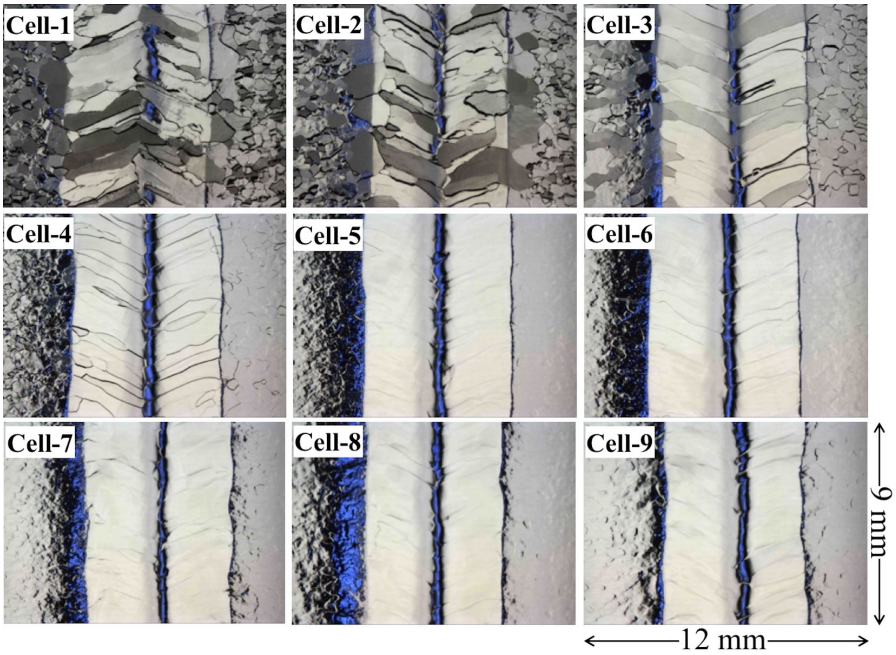

FIG. 10. Optical images of the equator surfaces after the VEP performed with initial parameters which were similar to those optimized for the single-cell cavity. Cell 1 represents the top cell in the VEP process. All the images have the same size of 12×9 mm.

The etched rough surface of the equator in the top four cells should be the result of a low electric field due to the strong cathode screening by a large quantity of H_2 gas bubbles. The surface was removed in the etching region instead of the plateau region in the $J-V$ curve. The etching was not caused by the temperature, because the temperature of the entire cavity was uniformly maintained. Bubbles were not only present in the cathode housing, but they probably diffused and accumulated in the upper cavity cell, which led to the strongly asymmetric removal.

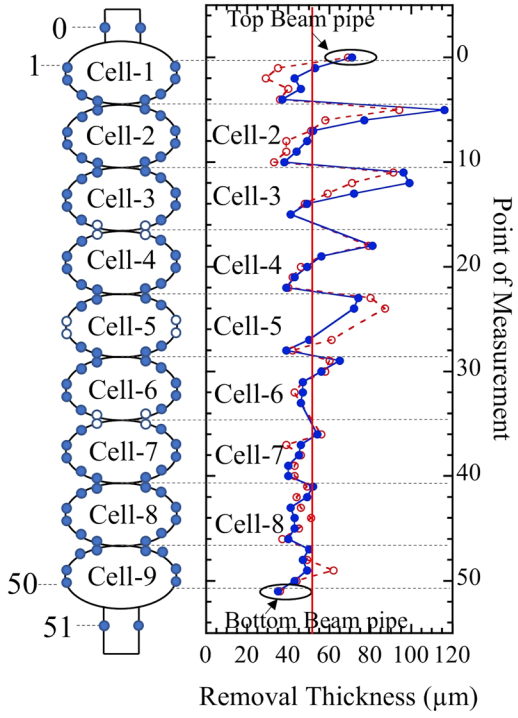

FIG. 11. Removal thickness along the cavity length in the VEP performed with parameters similar to those optimized for the single-cell cavity. The solid points in the schematic on the left show the positions where the thicknesses were measured. The vertical solid line shows the average removal thickness.

2. Parametric study with nine-cell coupon cavity

A VEP parametric study was carried out with the nine-cell coupon cavity to reveal the effect of cathode rotation, acid flow rate, temperature, and applied voltage on multi-cell cavities. Coupon currents were recorded as a function of the voltage and time under different conditions. The coupon currents shown in Fig. 12 were recorded for the acid flow rate of ~5 L/ min in the cavity and at a cavity temperature of ~15 °C. The equator and both iris coupon currents in the center and bottom cells were remarkably similar. The top iris coupon current in the top cell increased after 30–40 s of turning on the voltage and remained higher compared to the bottom iris and equator coupon currents in the cell. The top iris viewport in the top cell was observed, and videos were recorded from the viewport during the current measurements. The current increase was synchronized with the bubble accumulation on the viewport. The bubble density at the top side of the cathode housing was so high that the bubbles diffused from the housing to the upper cells of the cavity via the meshed sheet. As there was a large quantity of bubbles in the cell, the cathode rotation at 20 rpm could not make the coupon currents similar. However, it reduced the current difference.

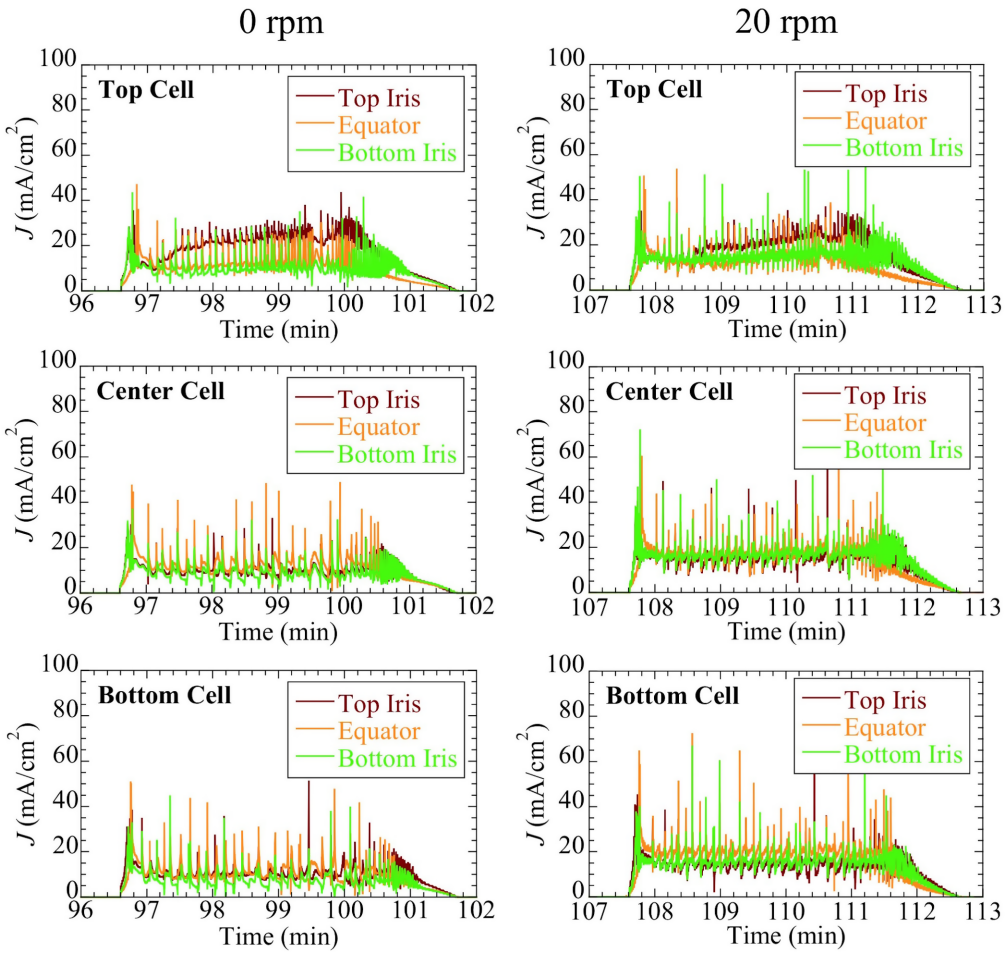

FIG. 12. Coupon currents in the top, center, and bottom cells at 0 (left) and 20 rpm (right). The acid flow was circulated at 5 L/ min, and the cavity temperature was set at ~15 °C in both tests.

As the 1.3 GHz nine-cell cavity has a high aspect ratio between the cavity length (~1270 mm long) and iris diameter (~73 mm), bubble removal from the cathode housing is slow. To remove the bubbles rapidly along the cathode with reduced diffusion from the cathode to the cavity and accumulation in the upper cavity cells, a novel acid flow technique called the dual-flow technique was developed. In this technique, an additional inlet was prepared to flow acid intentionally in the cathode housing. The acid inlet line was bifurcated to flow acid separately in the cavity and the cathode housing. The inlet system was designed with valves and flow meters to adjust the flow rates for the two lines, as shown in Fig. 3. Hereafter, the usual acid flow from the single inlet is called the single flow. The single and dual flows are illustrated by the schematics in Fig. 13.

The coupon currents and viewports were observed under different acid flow rates in the cavity and cathode housing. The applied flow conditions are listed in Table III. In the first three tests in the table, the flow rates in the cathode housing were set at 5, 10, and 20 L/ min, whereas the flow rate in the cavity was set to be ~5 L/ min. The coupon currents in the top cell under these conditions are shown in Fig. 14. The top iris coupon current was measured to be higher than the equator and bottom iris coupon currents when the flow rate in the cathode housing was ~5 L/ min. The top iris coupon current became remarkably similar to those of the other two coupons at the flow rate of ~10 L/ min. A higher flow rate of 20 L/ min further enhanced the top iris coupon current. The adequate flow rate of ~10 L/ min in the cathode housing and ~5 L/ min in the cavity (a total flow rate of ~15 L/ min) significantly reduced the bubble accumulation in the top cell. Two pictures of the viewport located near the top iris in the top cell are shown for the single flow at 5 L/ min and dual flow at the adequate flow rates in Fig. 15. The lower brightness of the backlight on the viewport in Fig. 15(a) was the result of the exceptionally large quantity of gas bubbles accumulated in the top cell.

The last two tests presented in Table III were conducted to compare the impact of the single and dual flow on the coupon currents without cathode rotation. In these tests, the single and dual flow were applied at the same total flow rate of 15 L/ min. The coupon currents in the top cell are shown

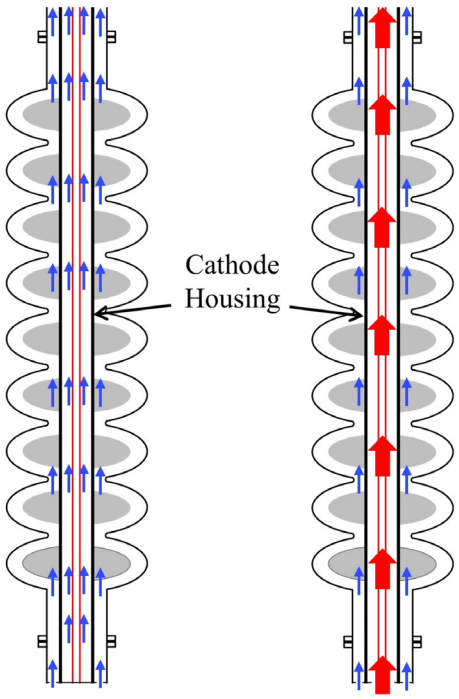

FIG. 13. Schematics of acid flow. Single flow (left): The acid flow in the cavity with no intentional flow in the cathode housing. Dual flow (right): The acid in the cavity and cathode housing using two different inlets. The red wide arrows represent the acid flow in the cathode housing.

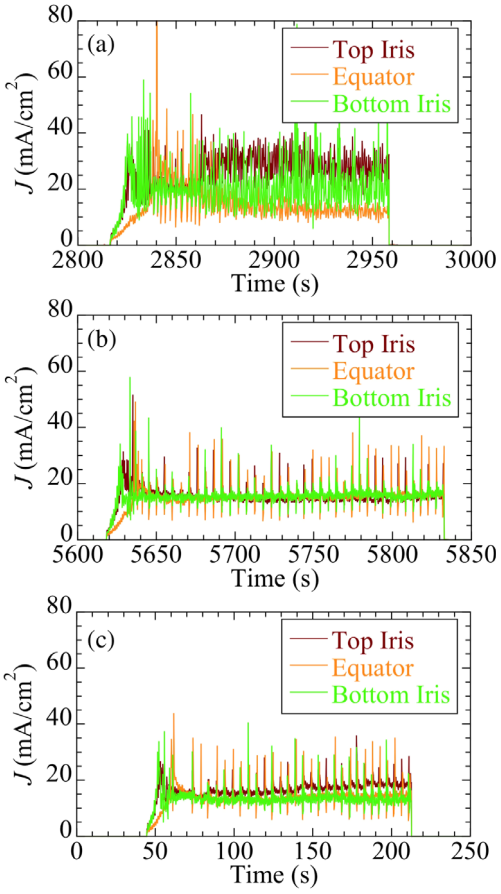

FIG. 14. Coupon currents in the top cell at a cathode rotation of 20 rpm, a cavity temperature of ~15 °C, and under the dual-flow condition, where the acid in the cavity is flowed at a rate of 5 L/ min and in the cathode housing at 5 (a), 10 (b), and 20 L/ min (c).

in Fig. 16. The difference between the top and bottom iris coupon currents was higher in the single flow. The result clearly shows that the dual flow is effective to yield similar coupon currents, which could be due to the efficient removal of bubbles from the cathode housing. A current difference in the dual flow at 0 rpm was also seen, because a small quantity of bubbles was always present in the cavity owing to the circulation of bubbles from the acid tank. A slight diffusion of bubbles from the cathode housing to the cavity might also occur. However, the bubble diffusion might be not strong, because a similar difference in the top and bottom iris coupon currents was noticed, even in the bottom cell. The effect of the dual flow was also monitored with a transparent plastic cavity, where a viscous colored liquid was flowed at different flow rates in the cathode housing while keeping a constant flow rate in the cavity. The colored liquid was flowing faster at a higher flow rate with a slight diffusion of the color in the cavity. The single acid flow with a higher flow rate might reduce the bubble accumulation in the cavity and make the currents similar. In this study, we have chosen the dual-flow method to be employed for the processing of the nine-cell cavity, because the effect of the dual flow was evident.

$J-V$ curves were obtained for the coupons and the cavity at a cathode rotation of 20 rpm, a temperature of ~15 °C, and with the optimized dual flow, as shown in

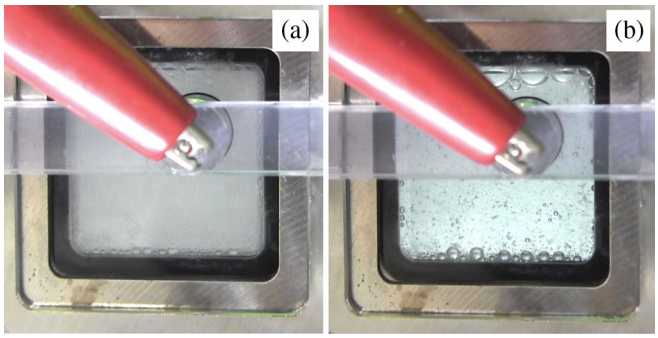

FIG. 15. Two pictures of the viewport near the top iris in the top cell during VEP performed with (a) single flow at 5 L/ min and (b) dual flow at 5 L/ min in the cavity and 10 L/ min in the cathode housing. The cathode rotation was set at 20 rpm. The lower brightness of backlight in (a) is caused by the exceptionally large quantity of bubbles in the cell. The size of the viewport is 25 × 25 mm.

TABLE III. Conditions of acid flow in the nine-cell cavity and cathode housing under dual flow.

S. no.	Flow rate (L/ min)		Cathode rotation (rpm)
	Cavity	Cathode housing	
1	5	5	20
2	5	10	20
3	5	20	20
4	15	No intentional flow	0
5	5	10	0

Fig. 17. Similar to the single-cell cavity, the equator coupons have EP plateaus at a higher voltage compared to those for the iris coupons. The shift in the EP plateau for the equator position in the upper cells was comparatively larger.

The larger shift in the EP plateau at the equator in the top cell is also explained by the screening effect caused by the gas bubbles in the upper side of the cavity. The bubble density was obviously higher in the upper part of the cathode. The equator coupon current in the top cell was found to be more scattered with the single flow of 5 L/ min, with which the bubble quantity was larger. The shift in the EP plateaus for the iris coupons in the top cell was not significant, because the iris coupons were closer to the cathode as compared to the equator ones.

The effect of the temperature was evaluated by observing the $J-V$ curves for the coupons and cavity at different cavity temperatures of 13, 18, and 23 °C. The cathode

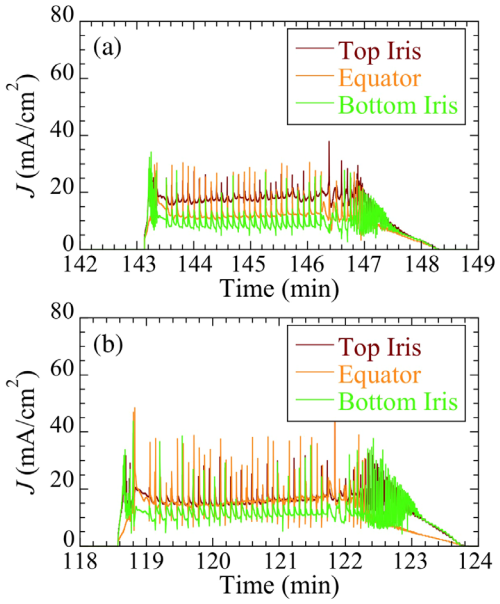

FIG. 16. Coupon currents in the top cell with single flow and dual flow at a cathode rotation of 0 rpm, cavity temperature of ~15 °C, and total flow rate of 15 L/ min. (a) Single flow at 15 L/ min and (b) dual flow at 5 L/ min in the cavity and 10 L/ min in the cathode housing.

rotation was set at 20 rpm, and the optimized dual flow was maintained during the tests. The EP plateaus for all the coupons shifted to a higher voltage side when the cavity temperature increased. The onset voltage for the EP plateau is shown against the cavity surface temperature in Fig. 18. The onset voltage for the equator coupons in the bottom and center cells linearly increased with the cavity temperature, whereas the onset voltage for the equator coupon in the top cell deviated from the linearity with a significantly higher value at a higher temperature. The nonlinear behavior was slightly reflected in the onset voltage for the cavity. The onset voltage for the cavity was found to be lower than that for the equator in the top cell. This reflects that the $J-V$ curve for the cavity does not show the correct onset voltage for the entire surface of the cavity. In this respect, the study with the nine-cell coupon cavity becomes important for finding an optimized voltage, which should be high enough for carrying out VEP for the entire cavity surface within the plateau region.

In a laboratory EP experiment performed for a small Nb sample [38], a shift in the EP plateau was not reported even up to a temperature of 39 °C. It may be due to no accumulation of gas bubbles around the cathode in beaker experiments, as the gas bubbles easily disperse in a beaker of a large volume. The shift in the plateaus in VEP is likely to be due to accumulation of gas bubbles in the cathode housing, where the gas bubbles screen the cathode surface to diminish the electric field. The higher temperature promoted the number density of gas bubbles in the cathode housing to enhance the onset voltage at a higher temperature. The average cavity current, which proportionally enhances the number of bubbles, was around 70% higher at 23 °C compared to that at 13 °C. The number density of gas bubbles is supposed to be the largest in the top cell. Therefore, the onset voltage in top cell showed nonlinear behavior with the cavity temperature. The results and discussion given here explain the results of the previous VEP performed for the cavity TB9-TSB02 with initial parameters (shown in Sec. III C 1). Obviously, according to the data in Fig. 18, the applied voltage in the VEP for TB9-TSB02 was lower than the onset voltage in the upper cells. This reveals that the rough surface of the upper cells of the TB9-TSB02 cavity are likely to be due to deteriorated EP conditions at the insufficient applied voltage. Based on the above study, the cavity temperature of ~15 °C was considered to be an optimized value to maintain the EP plateau well within 20 V. The operating temperature can be varied if the HF concentration is changed. A lower HF concentration reduces the total EP current [47] and, hence, lowers the screening effect. Therefore, it is possible to increase the operating temperature for VEP with a lower concentration of HF to maintain a similar current density of ~15 mA/cm^2.

The effect of VEP time was also observed on the coupon currents and accumulation of bubbles in the cavity cells.

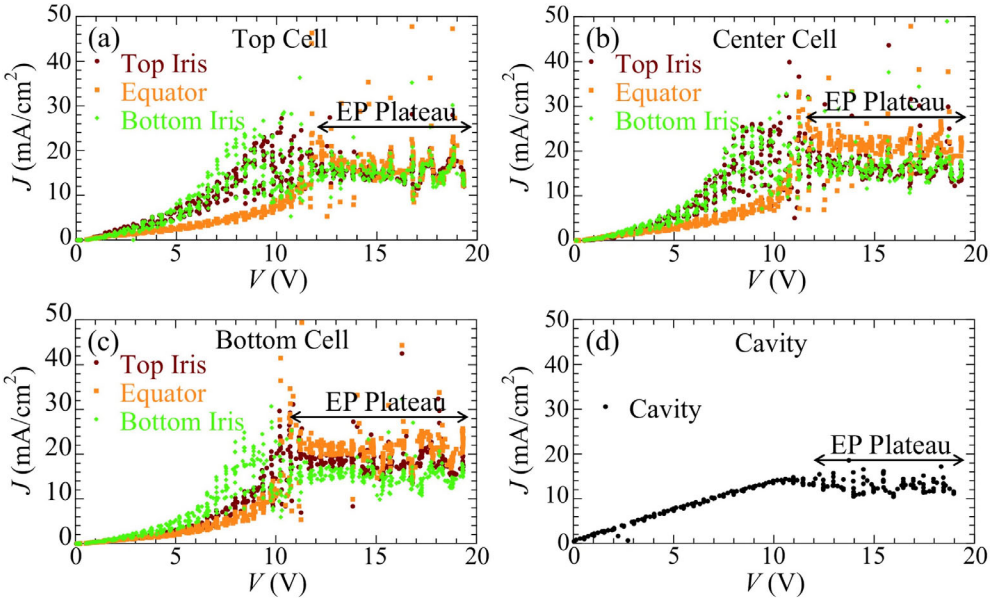

FIG. 17. Polarization ($J-V$) curves measured for the coupons in the top cell (a), center cell (b), bottom cell (c), and the cavity (d). Cathode rotation of 20 rpm and the optimized dual-flow condition were set during the measurement. The cavity temperature was uniformly maintained at ~15 °C.

The top iris coupon current in the bottom cell started increasing after 3 min of continuous VEP. It was monitored from the viewports that bubbles returned from the acid tank to the cavity. The returning bubbles accumulated in the bottom cell and enhanced the top iris coupon current in the cell. The circulation of bubbles occurred due to the small size of the acid tank, which had a capacity of 70 L. When the acid is flowed at 15 L/ min during VEP, the generated bubbles accumulate in the tank and finally move back to the cavity. This phenomenon was not noticed at a slower acid flow rate of less than 10 L/ min. The bubbles in the tank had sufficient time to be discharged from the acid at the slow flow rate. To reduce the bubble circulation at 15 L/ min, on-off voltage cycles with on and off periods of 3 min were preferred for VEP.

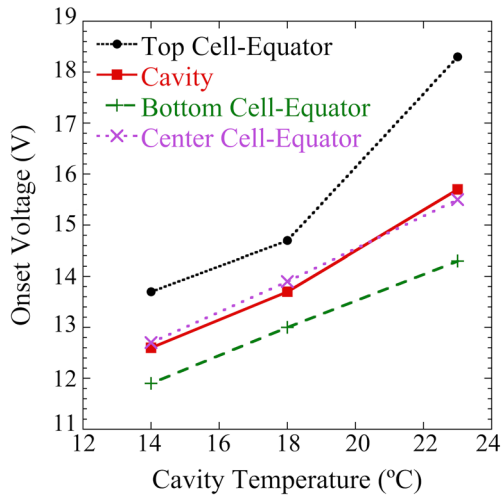

FIG. 18. Onset voltage, representing the minimum voltage at which the EP plateau appears, against the cavity surface temperature for the equator coupons and cavity. The tests were conducted with a cathode rotation of 20 rpm and optimized dual-flow condition.

VEP of the coupon cavity was performed with the dual-flow technique and the optimized parameters based on the above-mentioned parametric studies. The applied parameters for the VEP are listed in Table IV. A voltage (17.5 V) was applied with on-off cycles, where the on and off times were set to be 3 min. The cavity temperature was maintained well below 15 °C during the VEP test that lasted approximately 4 h, including the voltage-off period. Figure 19 shows the current and cavity temperature for two voltage cycles. The surface was EPed for an average removal of 25 μm. The EP rate calculated from the integrated current with the consideration of the total time, including the voltage-off period, was 0.09 μm/ min.

TABLE IV. Parameters applied for VEP of the nine-cell coupon cavity.

Condition	Value
Acid flow type	Dual flow
Flow rate in cathode housing	10 L/ min
Flow rate in cavity	5 L/ min
Cathode type	NC-4
Cathode rotation	20 rpm
Cavity temperature	<15 °C
Voltage	17.5 V
Voltage-on or -off period	3/3 min

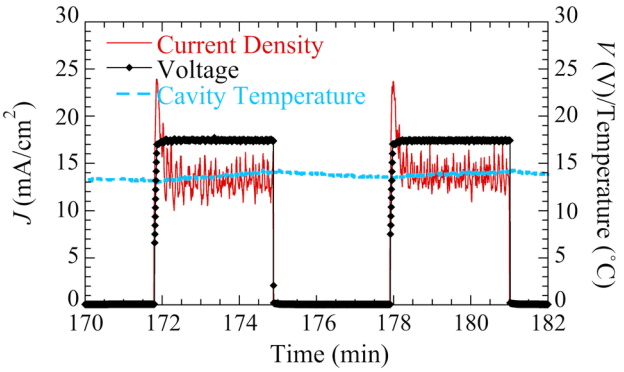

FIG. 19. Current, temperature, and voltage profiles in VEP of the nine-cell coupon cavity under a dual flow of acid and at a cathode rotation of 20 rpm.

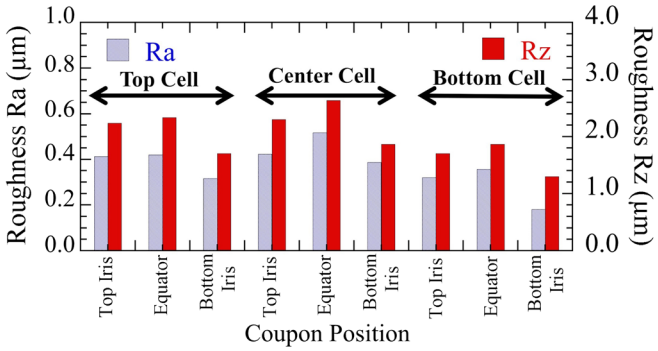

FIG. 21. Roughness Ra and Rz of the nine coupon surfaces after the VEP performed for an average removal thickness of ~25 μm.

The coupon surfaces after the VEP appeared smooth and lustrous in a visual inspection. The coupon surfaces, which represent the cavity surface at the coupon positions, were studied with SEM and the surface profiler to compare the surface state at different positions of the cavity. The SEM images and the roughness (Ra and Rz) of the coupon surfaces are shown in Figs. 20 and 21, respectively. The images and roughness values reveal that the coupon surfaces in the upper cells were comparatively rougher than the surfaces in the bottom cell. Fine bubble traces were observed on the top iris coupon surfaces of the upper cells. The fine bubble traces seem to be responsible for the higher roughness of the iris coupons in the top and center cells. However, these traces were not as deep as they usually are, with Rz of more than 10 μm after a VEP process performed with the conventional rod cathode [35]. In each voltage-on period of 3 min, the current was higher for less than 15 s, followed by a constant current. When the voltage is turned on, it takes some time in the formation of the diffusion layer for EP under the current limiting condition. All nine coupon surfaces might experience etching for less than 15 s in the absence of a diffusion layer and subsequent EP for the remaining period. As the EP time duration was much longer than the etching duration, the impact of the

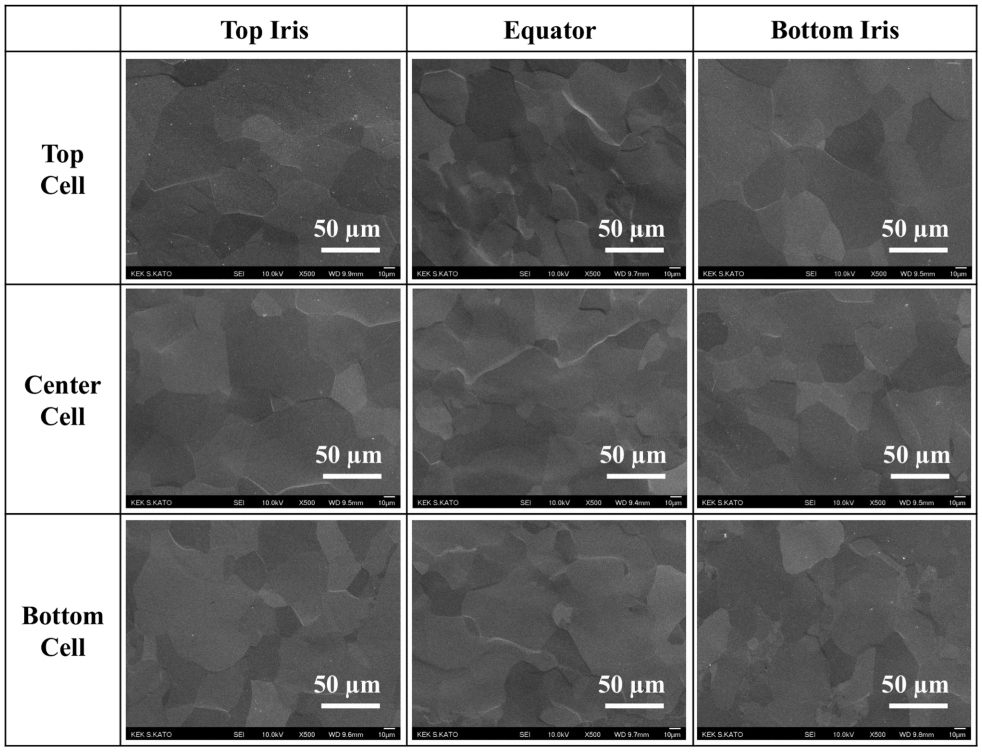

FIG. 20. SEM images of the coupons from the nine-cell coupon cavity after VEP performed for average removal of 25 μm with the dual-flow method, a cathode rotation of 20 rpm, and a cavity temperature of ~15 °C.

TABLE V. Details of the HEP and VEP treatments applied to three nine-cell cavities used for a comparison of removal trends and surface morphologies.

Cavities	Pretreatment	Current treatment	EP parameters for current treatment
TB9-TSB02	VEP (51 μm)	VEP (20 μm)	See Table IV (voltage, 18.5 V)
TB9-TSB01	HEP (100 + 30 μm)	VEP (100 μm)	See Table IV (voltage, 18.5 V)
TB9-MHI01	HEP sequences	HEP (40 μm)	Acid flow rate, 15 L/ min; cavity temperature, 22–25 °C; voltage, 19 V; cavity rotation, 1 rpm

etching in the roughness might be not significant. The slightly rough equator surfaces in the upper cells indicated that the cathode screening effect was stronger in the upper side. An even higher voltage might overcome the effect of cathode screening to make the equator surface smoother in the upper cells. A larger acid tank with a capacity of a few hundred liters could reduce the circulating bubbles in the cavity, and a higher cathode rotation speed, e.g., 30–50 rpm, displaces the bubbles sticking on the surface. As a result of this, a smoother surface of the top iris is expected. The effect of 50 rpm has been already confirmed to displace bubbles from the upper half cell surface of the single-cell cavity [35]. The higher rotation will shift the EP plateaus by 1–2 V to the higher-voltage side. However, it can be compensated by applying a higher voltage. The large capacity tank will also make it possible to perform VEP continuously, without the voltage-off period. This will prevent the partial etching of the surface at the voltage turn-on in the voltage cycles. The continuous VEP will also double the EP rate, to 0.18 μm/ min, which is necessary for mass production.

3. Comparison of surface morphology and removal with HEP

A further study of the removal and surface morphology, in comparison to those obtained with HEP, was performed. Three 1.3 GHz Tesla shapelike nine-cell cavities were processed with VEP and HEP, as presented in Table V. The cavities (TB9-TSB02 and TB9-TSB01) were processed with VEP using the parameters optimized with the nine-cell coupon cavity. The voltage was slightly enhanced to 18.5 V in these VEP processes. The cavity TB9-TSB02 was pretreated with VEP under initial conditions as shown in Sec. III C 1, whereas the cavity TB9-TSB01 was pretreated with the standard HEP process in the STF/KEK. The cavity TB9-MHI01 was treated with HEP in the STF at the KEK. The removal rate with HEP was calculated to be 0.28 μm/ min, which was higher than the 0.1 μm/ min rate in the VEP performed with the on-off voltage cycles. However, VEP has an advantage over HEP in terms of a higher removal rate if the same temperature of ∼15 °C is used in both EP processes. The low-temperature EP is preferred to improve the surface smoothness [48] and reduce H_2 absorption in Nb bulk [49].

The removal trends were measured in the current VEP and HEP treatments of the three cavities. These three measurements are for different total removal amounts but provide general removal trends. The removal trends are compared in Fig. 22. In the VEP, the top iris showed higher removal compared to that on the bottom iris and equator in each cell. The difference in removal between the irises increases in the upper cells. In comparison to the removal trend shown in Fig. 11, the removal asymmetry was larger in the bottom four cells. However, the removal uniformity along the cavity in the VEP performed with the optimized parameters significantly improved as compared to the removal trend shown in Fig. 11. In HEP, the removal thickness at the irises was approximately twice that at the equator. Similar nonuniformity in HEP has been reported by other laboratories [50]. The irises of the center cell show higher removal compared to those of the other cells. The maximum removal difference in the HEP and VEP remains similar except the asymmetric removal in the cavity cells in VEP.

The asymmetry within the cells is supposed to be due to the bubbles, which were residing on the surface for a longer time and were not influenced by the cathode rotation at 20 rpm. These bubbles moved from the tank to the cavity, even in the voltage-off period, as the acid was continuously flowing during the VEP process, although the voltage-off period reduced the bubble circulation significantly. Given that the circulating bubbles enter from the bottom side, the removal asymmetry was also observed in the bottom cells. The removal in the four bottom cells was better in uniformity in the VEP performed with an acid flow rate of 5 L/ min, because bubble circulation was not seen at a slower flow rate. A small quantity of bubbles might also diffuse from the cathode housing to the cavity via the mesh covering the cathode housing. The diffusing bubbles might also contribute to the higher removal of the top irises. Both phenomena, circulating bubbles and bubble diffusion from the cathode housing, need to be separated. This can be accomplished when the circulation of bubbles is prevented by using a larger capacity of the acid tank. As stated above, a higher cathode rotation speed could displace the bubbles from the surface to stop the formation of bubble traces. It may also reduce the removal asymmetry in the cell. The higher removal on the irises of the nine-cell cavity in HEP is similar to that observed in the single-cell cavity.

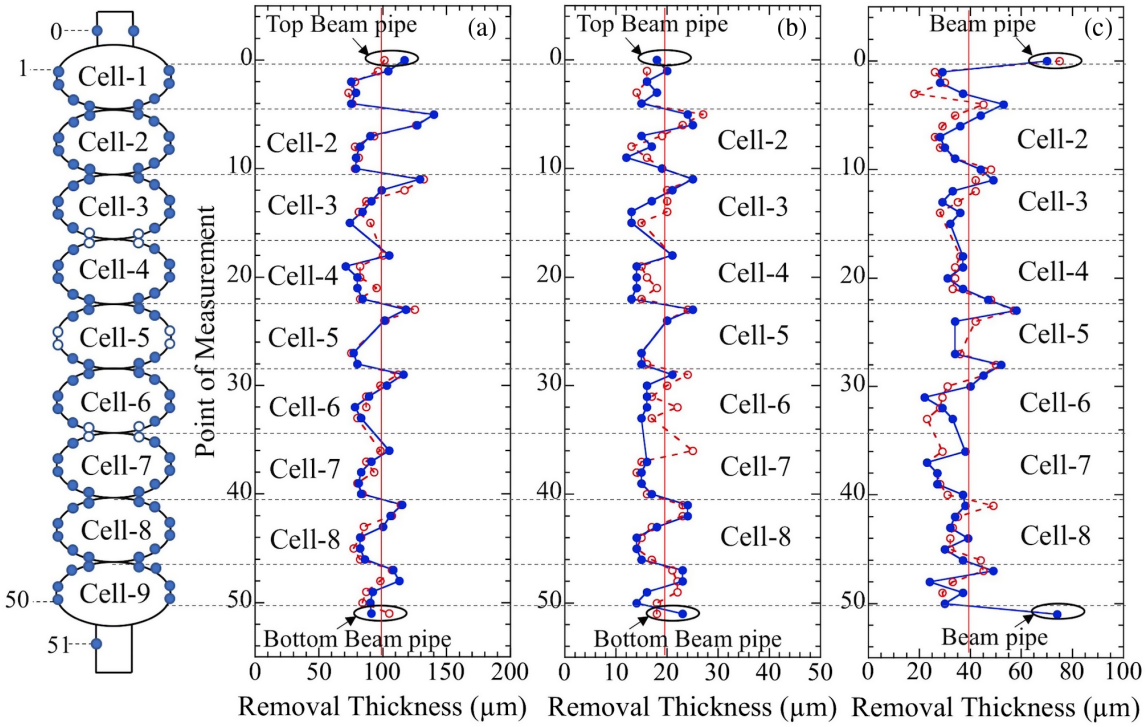

FIG. 22. Removal trends along the cavity length with VEP (a),(b) and with HEP (c) of nine-cell cavities. The solid dots on the schematic at the left represent the positions of thickness measurement. The vertical lines represent the average removal of the cavities.

Furthermore, in the nine-cell cavity, the higher removal on the irises might be related to a higher acid flow on them.

The equator surfaces before and after the VEP performed with the optimized parameters were compared. The etched equator surface in the top cells of the TB9-TSB02 cavity turned out to be smoother after the VEP performed with the optimized conditions. Figure 23 shows the surfaces at the same equator positions of the TB9-TSB01 cavity before and after the bulk removal in the VEP, where the surface before the VEP represents the HEP treated surface. The surfaces in all the cells after the VEP were found to be similar to the initial HEPed surface. The smooth surface confirms that the parameters optimized with the coupon cavity are applicable to bulk removal.

4. Field flatness

Every cell of a multicell cavity needs to be tuned at the designed resonant frequency to attain the same field in the cavity cells for the maximum accelerating field [1]. In this study, the field flatness was measured using the bead-pull method for the TB9-TSB02 and TB9-TSB01 cavities treated with VEP using the initial and optimized parameters. The field flatness before and after the VEP treatments is summarized in Table VI. The results reveal that the field flatness was significantly degraded after the VEP performed with initial parameters. The degradation in the field flatness might be related to the asymmetric and higher average removal as measured in the top five cells of the

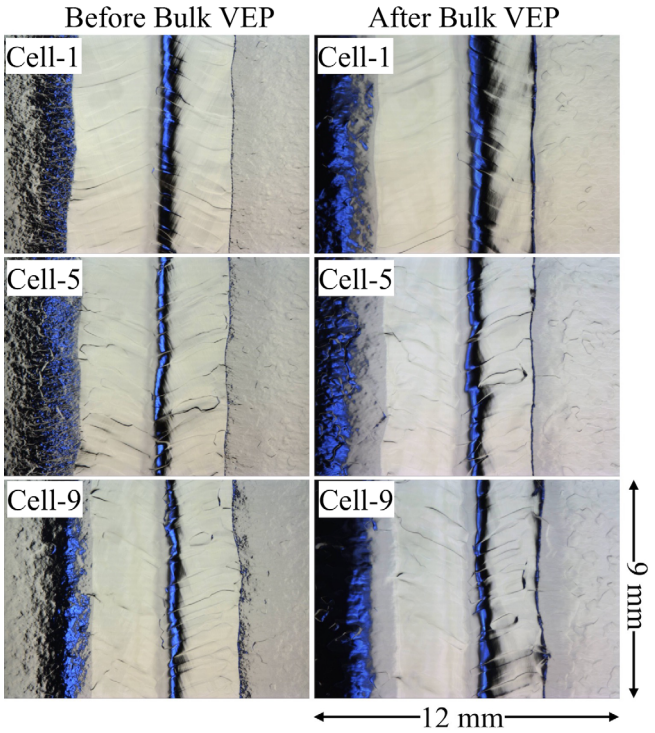

FIG. 23. Equator surfaces in the top, center, and bottom cells of the TB9-TSB01 cavity before (left images) and after (right images) bulk VEP for 100 μm removal. The same positions of the equator are compared. Cell 1 represents the top cell. All the images have the same scale.

TABLE VI. Field flatness of the cavity after VEP of TB9-TSB02 and TB9-TSB01 cavities under initial and optimized VEP conditions.

Cavity	VEP condition	Removal thickness (μm)	Field flatness before VEP (%)	Field flatness after VEP (%)
TB9-TSB02	Initial	51	91	67
TB9-TSB02	Optimized	20	97	98
TB9-TSB01	Optimized	100	95	91
TB9-TSB01	Optimized	10	99	99

TB9-TSB02 cavity. The maximum reduction in the field amplitude of the order of ~25% was observed in the top cell, which was EPed with strongly asymmetric and higher average removal than that in the lower cells. The flatness was reduced only by a few percent, even after the bulk removal of 100 μm in VEP performed with the optimized parameters. Such degradation is also observed after the bulk removal with HEP treatments and was attributed to the higher average removal in the end cells [51]. The field flatness was not altered after the light removal of 10 and 20 μm in VEP. In the case of the low average removal of 20 μm in VEP, all the cells show a similar removal trend, with almost similar average removal in each cell [see Fig. 22(b)]. This similar removal in each cell might result in the unaltered field flatness after VEP for 10 and 20 μm removal. This suggests that, like in cavity treatment with HEP [49], a light removal of ~20 μm could be chosen for the final treatment of the cavities with VEP to avoid degradation in the field flatness.

D. rf test of TB9-TSB01 cavity

A vertical test of the TB9-TSB01 cavity for measurement of the SRF performance at 2 K was carried out after the sequence of three VEP steps for 100, 20, and 10 μm removal. The VEP was conducted with the optimized parameters. The cavity was annealed at 750 °C after 100 and 20 μm removal. The cavity was treated for light removal of 10 μm followed by high-pressure water rinsing (HPR) and baking at 120 °C for 48 h before the vertical test was performed. The maximum E_{acc} of 28.3 MV/m and a Q_0 value of 6.7×10^9 were achieved in the π mode. The Q_0 (E_{acc}) performance is compared with the baseline rf performance obtained after the HEP treatment and 120 °C baking of the same cavity (see Fig. 24). In the HEP process also, the cavity was EPed for bulk removal of 100 μm followed by annealing at 750 °C, light removal of 30 μm, HPR, and baking at 120 °C. The cavity after the VEP treatment showed the same performance as that achieved after the HEP treatment. In both tests, the cavity performance was limited by the quench that occurred at different positions.

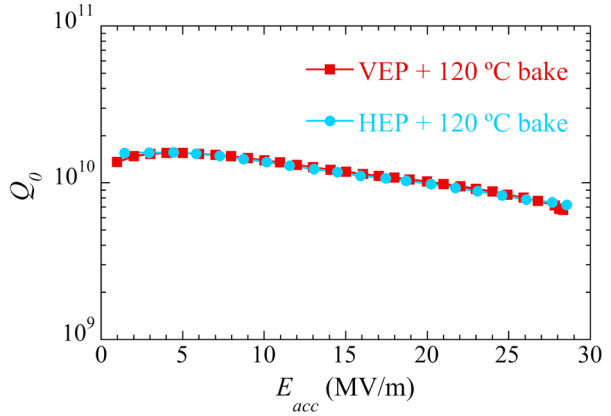

FIG. 24. SRF performances (Q_0 versus E_{acc} curves) of cavity TB9-TSB01 at 2 K in vertical tests after an average removal of 130 μm, including bulk and light removals, in both HEP and VEP processes. The tests were performed after post-light EP baking at 120 °C for 48 h.

IV. CONCLUSION

The present parametric study was performed using a unique cathode with single- and nine-cell coupon cavities to optimize the VEP parameters with the aim to attain a uniform removal and smooth surface in the interior of the cavities. The cathode designed with the meshed housing along with optimized parameters including voltage, temperature, acid flow rate, and cathode rotation speed resulted in the desired smooth surface and uniform removal in the single-cell cavities. The single-cell cavity (TB1-TSB02) tested in the vertical cryostat showed the same rf performance as that achieved after the standard HEP method. However, the parameters optimized for the single-cell cavity yielded a strongly asymmetric removal and a rough surface in the upper cells of the nine-cell cavity. The removal in the upper cells was the result of etching rather than of a diffusion process. The results revealed the existence of strong screening of the cathode surface by the exceptionally large quantity of bubbles in the upper part of the cathode housing and upper cells of the cavity. To remove the H_2 gas bubbles efficiently from the nine-cell cavity, the dual-flow method was applied to flow the acid in the cathode housing and cavity separately. The flow rates of 10 L/ min in the cathode housing and 5 L/ min in the cavity were optimized while observing the coupon currents, mainly in the top cell. Additionally, the on-off voltage cycles with the same on and off periods of 3 min were

chosen for VEP where the off-voltage period was found necessary to reduce the gas bubbles returning from the acid tank to the cavity. The asymmetric removal and surface roughness were significantly lowered with the dual-flow method, along with the optimized temperature and voltage required for a diffusion-limited removal. The nine-cell cavity TB9-TSB01 after bulk and light removals with the VEP process showed as good of a superconducting rf performance at 2 K as that achieved after the HEP process of the same cavity. The results are promising and reveal that the VEP process could be an alternative technique of the standard HEP technique for 1.3 GHz nine-cell Nb SRF cavities. The smooth surface and good SRF performance after VEP for the bulk removal, which was enough to initialize the surface, show that a pristine cavity can be processed with the VEP parameters optimized in this work. However, the removal rate, which is $\sim 0.1\ \mu\mathrm{m}/\mathrm{min}$ with on-off voltage cycles, needs to be improved to make the VEP process feasible for mass production. More experiments are planned with a larger capacity of the acid tank, which can stop the circulation of bubbles. A continuous voltage could be applied once the bubble circulation is stopped. A VEP operation with continuous voltage would obviously double the removal rate. Further improvement in the removal uniformity and surface smoothening in the nine-cell cavity is also expected with the larger tank in combination with a higher cathode rotation speed and a higher voltage.

ACKNOWLEDGMENTS

We thank two Japanese companies, WING Co., Ltd., Japan, and Higashinihon Kidenkaihatsu Co. Ltd., Japan, for their support in development and automation of the VEP system.

[1] H. Padamsee, J. Knobloch, and T. Hays, *RF Superconductivity for Accelerators* (Wiley, New York, 1998).

[2] H. Padamsee, The science and technology of superconducting cavities for accelerators, Supercond. Sci. Technol. **14**, R28 (2001).

[3] V. Palmieri, F. Stivanello, S. Yu. Stark, C. Roncolato, and M. Valentino, Besides the standard niobium bath chemical polishing, in *Proceedings of the 10th Workshop on RF Superconductivity* (KEK, Tsukuba, Japan, 2001), pp. 408–412.

[4] H. Diepers, O. Schmidt, H. Martens, and F. Sun, A new method of electropolishing niobium, Phys. Lett. **37A**, 139 (1971).

[5] L. Lilje, E. Kako, D. Kostin, A. Matheisen, W.-D. Moller, D. Proch, D. Reschke, K. Saito, P. Schmuser, S. Simrock, T. Suzuki, and K. Twarowski, Achievement of 35 MV/m in the superconducting nine-cell cavities for TESLA, Nucl. Instrum. Methods Phys. Res., Sect. A **524**, 1 (2004).

[6] A. Aspart and C. Z. Antoine, Study of the chemical behavior of hydrofluoric, nitric and sulfuric acids mixtures applied to niobium polishing, Appl. Surf. Sci. **227**, 17 (2004).

[7] A. C. Crawford, Extreme diffusion limited electropolishing of niobium radiofrequency cavities, Nucl. Instrum. Methods Phys. Res., Sect. A **849**, 5 (2017).

[8] H. Tian, S. G. Corcoran, C. E. Reece, and M. J. Kelley, The mechanism of electropolishing of niobium in hydrofluoric–sulfuric acid electrolyte, J. Electrochem. Soc. **155**, D563 (2008).

[9] H. Tian and C. E. Reece, Evaluation of the diffusion coefficient of fluorine during the electropolishing of niobium, Phys. Rev. Accel. Beams **13**, 083502 (2010).

[10] F. Eozenou, S. Berry, C. Antoine, Y. Gasser, J.-P. Charrier, and B. Malki, Aging of the HF-H_2SO_4 electrolyte used for the electropolishing of niobium superconducting radio frequency cavities: Origins and cure, Phys. Rev. Accel. Beams **13**, 083501 (2010).

[11] K. Saito, H. Inoue, E. Kako, T. Fujino, S. Noguchi, M. Ono, and T. Shishido, Superiority of electropolishing over chemical polishing on high gradients, in *Proceedings of the 8th Workshop on RF Superconductivity (SRF1997), Abano Terme Padova, Italy, 1997* (IFN, Padova, Italy, 1998), pp. 795–813.

[12] K. Saito *et al.*, R&D of superconducting cavities at KEK, in *Proceedings of the 4th Workshop on RF Superconductivity* (KEK, Tsukuba, Japan, 1989), pp. 635–694.

[13] E. Kako, S. Noguchi, M. Ono, K. Saito, T. Shishido, B. Aune, J.-P. Charrier, M. Juillard, and H. Safa, Improvement of cavity performance by electropolishing in the 1.3 GHz Nb superconducting cavities, in *Proceedings of the 18th Particle Accelerator Conference, New York, 1999* (IEEE, New York, 1999), pp. 432–434.

[14] K. Saito, Techniques of SC cavity performance for high gradient, in *Proceedings of the XXI Linear Accelerator Conference (LINAC2002), Gyeongju, Korea, 2002* (Pohang Accelerator Laboratory, Pohang, Korea, 2002), pp. 534–538.

[15] R. L. Geng, S. Castagnola, A. C. Crawford, D. Forehand, B. Golden, C. Reece, and S. Williams, Improving gradient and Q performance of BCP etched multi-cell cavities by applying a light EP, in *Proceedings of the 14th Workshop on RF Superconductivity (SRF2009), Berlin, Germany, 2009* (Helmholtz Zentrum für Materialien und Energie, Berlin, 2009), pp. 735–737.

[16] G. Ciovati, G. Myneni, F. Stevie, P. Maheshwari, and D. Griffis, High field Q slope and the baking effect: Review of recent experimental results and new data on Nb heat treatments, Phys. Rev. Accel. Beams **13**, 022002 (2010).

[17] H. Padamsee, *RF Superconductivity: Science, Technology and Applications* (Wiley-VCH Verlag, Weinheim, 2009), p. 142.

[18] R. L. Geng, J. Knobloch, and H. Padamsee, Microstructures of RF surfaces in the electron-beam-weld regions of niobium, in *Proceedings of the 1999 Workshop on RF Superconductivity, Santa Fe, NM, 1999* (CERN, Geneva, 1999), pp. 238–245.

[19] J. Knobloch, R. L. Geng, M. Liepe, and H. Padamsee, High-field Q slope in superconducting cavities due to magnetic field enhancement at grain boundaries, in *Proceedings of the 1999 Workshop on RF Superconductivity, Santa Fe, NM, 1999* (CERN, Geneva, 1999), pp. 77–91.

[20] K. Saito, Development of electropolishing technology for superconducting cavities, in *Proceedings of the 2003 Particle Accelerator Conference, Portland, OR* (IEEE, New York, 2003), pp. 462–466.

[21] C. E. Reece, A. C. Crawford, and R. L. Geng, Improved performance of JLAB 7-cell cavities by electropolishing, in *Proceedings of the 23rd Particle Accelerator Conference, Vancouver, Canada, 2009* (IEEE, Piscataway, NJ, 2009), pp. 2126–2128.

[22] C. Cooper, J. Brandt, L. Cooley, M. Ge, E. Harms, T. Khabiboulline, and J. Ozelis, Recent developments in electropolishing and tumbling R&D at Fermilab, in *Proceedings of the 14th Workshop on RF Superconductivity (SRF2009), Berlin, Germany, 2009* (Helmholtz Zentrum für Materialien und Energie, Berlin, 2009), pp. 806–810.

[23] T. Reid, P. N. Ostroumov, M. P. Kelly, Z. A. Conway, S. M. Gerbick, and M. Kedzie, Electropolishing for low-beta and quasi-waveguide SRF cavities, in *Proceedings of the 6th International Particle Accelerator Conference (IPAC2015), Richmond, VA* (JACoW, Geneva, Switzerland, 2015), pp. 3273–3275.

[24] S. C. Joshi, S. Raghavendra, V. K. Jain, A. Puntambekar, P. Khare, J. Dwivedi, G. Mundra, P. K. Kush, P. Shrivastava, S. B. Roy, P. R. Hannurkar, and P. D. Gupta, Development of superconducting cavities and related infrastructure for high intensity proton LINAC for spallation neutron source, in *Proceedings of the 27th Linear Accelerator Conference (LINAC2014), Geneva, Switzerland, 2014* (JACoW, Geneva, Switzerland, 2014), pp. 1140–1143.

[25] R. L. Geng, C. Crawford, H. Padamsee, and A. Seaman, Vertical electropolishing niobium cavities, in *Proceedings of the 12th International Workshop on RF Superconductivity (SRF2005)* (Cornell University, Ithaca, 2005), pp. 459–463.

[26] H. Padamsee, A. C. Crawford, A. Favale, M. Cole, J. Rathke, M. Pekeler, and B. Ashmanskas, Results on 9-cell ILC and 9-cell re-entrant cavities, in *Proceedings of 22nd Particle Accelerator Conference, Albuquerque, NM, 2007* (IEEE, New York, 2007), pp. 2343–2345.

[27] F. Furuta, G. Hoffstaetter, M. Liepe, B. Elmore, and D. Krebs, Cornell VEP update, VT results and R&D on Nb coupon, in *Proceedings of the 16th International Workshop on RF Superconductivity (SRF2013), Paris, France, 2013* (IN2P3, Paris, 2014), pp. 524–526.

[28] F. Furuta *et al.*, Vertical electropolishing studies at Cornell, in *Proceedings of the 17th International Workshop on RF Superconductivity (SRF2015), Whistler, Canada, 2015* (JACoW, Geneva, Switzerland, 2015), pp. 364–367.

[29] S. Calatroni, L. Ferreira, M. Macatrao, A. Skala, M. Sosin, R. de Waele, and Y. Withofs, Status of EP simulations and facilities for the SPL, in *Proceedings of the 25th Linear Accelerator Conference (LINAC 2010), Tsukuba, Japan, 2010* (KEK, Tsukuba, Japan, 2010), pp. 824–826.

[30] F. Eozenou, S. Chel, Y. Gasser, C. Servouin, B. Visentin, and J-P. Charrier, and Z. Wang, Development of an advanced electropolishing setup for multicell high gradient niobium cavities, Phys. Rev. Accel. Beams **15**, 083501 (2012).

[31] A. M. Rowe, A. Grassellino, T. D. Hall, M. E. Inman, S. T. Snyder, and E. J. Taylor, Bipolar EP: Electropolishing without fluorine in a water based electrolyte, in *Proceedings of the 16th International Workshop on RF Superconductivity (SRF2013), Paris, France, 2013* (IN2P3, Paris, 2014), pp. 401–406.

[32] H. Tian, L. Phillips, J. Musson, C. Seaton, M. Lester, and C. E. Reece, Commissioning of JLab vertical cavity processing system for SRF Nb single cell and multi-cell cavity with HF-free pulse-reversed electropolishing, in *Proceedings of 9th International Particle Accelerator Conference (IPAC2018), Vancouver, Canada, 2018* (JACoW, Geneva, Switzerland, 2018), pp. 3978–3981.

[33] F. Furuta, M. Ge, T. Gruber, J. Kaufman, P. Koufalis, J. Sears, M. Liepe, T. Hall, M. Inman, E. J. Taylor, R. Radhakrishnan, and S. Snyder, HF free bipolar electropolishing studies on niobium SRF cavities at Cornell with Faraday technology, in *Proceedings of 9th International Particle Accelerator Conference (IPAC2018), Vancouver, Canada, 2018* (JACoW, Geneva, Switzerland, 2018), pp. 2443–2446.

[34] F. Eozenou, Y. Boudigou, P. Carbonnier, J-P. Charrier, Y. Gasser, L. Maurice, F. Peauger, D. Roudier, C. Servouin, and K. Muller, Development of vertical electropolishing process applied on 1300 and 704 MHz superconducting niobium resonators, Phys. Rev. Accel. Beams **17**, 083501 (2014).

[35] V. Chouhan, S. Kato, K. Nii, T. Yamaguchi, M. Sawabe, H. Hayano, and Y. Ida, Effort towards symmetric removal and surface smoothening of 1.3 GHz niobium single-cell cavity in vertical electropolishing using a unique cathode, Phys. Rev. Accel. Beams **20**, 083502 (2017).

[36] S. Jin, A. T. Wu, X. Y. Lu, R. A. Rimmer, L. Lin, K. Zhao, J. Mammosser, and J. Gao, Effect of cathode shape on vertical buffered electropolishing for niobium SRF cavities, Appl. Surf. Sci. **280**, 93 (2013).

[37] C. Boffo, P Bauer, T. Reid, and R. Geng, Electropolishing of small samples at Fermilab, in *Proceedings of the 12th International Workshop on RF Superconductivity (SRF2005)* (Cornell University, Ithaca, 2005), pp. 447–450.

[38] N. W. Khun, M. Sumption, and G. S. Frankel, Smoothening of niobium by electropolishing, J. Appl. Electrochem. **43**, 829 (2013).

[39] V. Chouhan, Y. Ida, K. Ishimi, K. Nii, T. Yamaguchi, H. Hayano, S. Kato, H. Monjushiro, T. Saeki, and M. Sawabe, Recent development in vertical electropolishing, in *Proceedings of the 17th International Workshop on RF Superconductivity (SRF2015), Whistler, Canada, 2015* (JACoW, Geneva, Switzerland, 2015), pp. 1024–1030.

[40] P. V. Tyagi, M. Nishiwaki, T. Saeki, M. Sawabe, H. Hayano, T. Noguchi, and S. Kato, Surface analyses of electropolished niobium samples for superconducting radio frequency cavity, J. Vac. Sci. Technol. A **28**, 634 (2010).

[41] A. Navitski, E. Elsen, B. Foster, A. Prudnikava, and Y. Tamashevich, Surface analyses and optimization of centrifugal barrel polishing of Nb cavities, in *Proceedings of the 17th International Workshop on RF Superconductivity (SRF2015), Whistler, Canada, 2015* (JACoW, Geneva, Switzerland, 2015), pp. 286–290.

[42] S. Kato, H. Hayano, H. Inoue, H. Monjushiro, T. Saeki, M. Sawabe, V. Chouhan, Y. Ida, K. Nii, and T. Yamaguchi,

Fabrication of 9 cell coupon cavity for vertical electropolishing test, in *Proceedings of the 28th International Linear Accelerator Conference (LINAC2016), East Lansing, MI, 2016* (JACoW, Geneva, Switzerland, 2017), pp. 220–222.

[43] L. M. A. Ferreira, H. Rana, and J. A. Shirra, Electropolishing simulation on full scale radio frequency elliptical structures, in *Proceedings of the 27th Linear Accelerator Conference (LINAC2014), Geneva, Switzerland, 2014* (JACoW, Geneva, Switzerland, 2014), pp. 898–900.

[44] J. J. Keir, P. R. Harmer, D. Lang, R. E. Laxdal, T. Shishido, R. Smith, and T. Shishido, Vertical electro-polishing at TRIUMF, in *Proceedings of the 17th International Workshop on RF Superconductivity (SRF2015), Whistler, Canada* (JACoW, Geneva, Switzerland, 2015), pp. 378–380.

[45] M. Bruchon, B. Visentin, and F. Eozenou, Electropolishing on single and multi-cell: COMSOL modelling, in *Proceedings of the 13th International Workshop on RF Superconductivity (SRF2007), Beijing, China, 2007* (Peking University, Beijing, 2009), pp. 247–250.

[46] Y. Iwashita and Y. Tajima, Development of high resolution camera for observations of superconducting cavities, Phys. Rev. ST Accel. Beams **11**, 093501 (2008).

[47] H. Tian, S. G. Corcoran, M. J. Kelley, and C. E. Reece, Novel characterization of the electropolishing of niobium with sulfuric and hydrofluoric acid mixtures, in *Proceedings of the 13th International Workshop on RF Superconductivity (SRF2007), Beijing, China, 2007* (Peking University, Beijing, 2009), pp. 370–376.

[48] C. E. Reece and H. Tian, Exploiting new electrochemical understanding of niobium electropolishing for improved performance of SRF cavities for CEBAF, in *Proceedings of the 25th International Linear Accelerator Conference (LINAC-2010), Tsukuba, Japan* (KEK, Tsukuba, Japan, 2010), pp. 779–781.

[49] H. Padamsee, *RF Superconductivity: Science, Technology and Applications* (Wiley-VCH Verlag, Weinheim, 2009), pp. 66–69.

[50] TTC-Report No. 2008-05, Final surface preparation for superconducting cavities, http://flash.desy.de/sites/site_vuvfel/content/e403/e1644/e2271/e2272/infoboxContent2354/TTC-Report2008-05.pdf.

[51] F. Marhauser, J. Follkie, and C. E. Reece, Investigation of differential surface removal due to electropolishing at Jlab, in *Proceedings of the 6th International Particle Accelerator Conference (IPAC2015), Richmond, VA* (JACoW, Geneva, Switzerland, 2015), pp. 3525–3527.